A Microscopic Gibbs Field Model for the Macroscopic Behavior of a Viscoplastic Fluid

UCDMS Research Report 2014/1 (Version Date: *August 25 2014*)

Raazesh Sainudiin[a], Miguel Moyers-Gonzalez[a], and Teodor Burghelea[b]

[a]*School of Mathematics and Statistics, Private Bag 4800, University of Canterbury, Christchurch 8041, New Zealand*
[b]*Université de Nantes, Nantes Atlantique Universités, CNRS, Laboratoire de Thermocinétique de Nantes, UMR 6607, La Chantrerie, Rue Christian Pauc, B.P. 50609, F-44306 Nantes Cedex 3, France*

Abstract

We present a Gibbs random field model for the microscopic interactions in a viscoplastic fluid. The energy function is derived from the Gibbs potential in terms of the external stress and internal energy. The resulting Gibbs distribution, over a configuration space of microscopic interactions, can mimic experimentally observed macroscopic behavioral phenomena that depend on the externally applied stress. A simulation algorithm that can be used to approximate samples from the Gibbs distribution is given and it is used to gain several insights about the model. The model has two parameters for the internal energy of the material in the absence of external stress and a third parameter for a constant externally applied stress. An approximating differential equation for the expected proportion of the material in the solid phase is derived by a spatio-temporal rescaling of the toroidal square lattice upon which the Gibbs random field model is defined. The asymptotic dynamics of this tri-parametric family of differential equation matches with those of the rescaled simulations from the Gibbs field model and can account for the macroscopic behaviors, including solid-fluid phase transitions in the presence of constant as well as varying external stress and the associated hysteresis.

Keywords: Gibbs Field, Interacting Particle System, Approximating Differential Equation

1. Introduction

Yield stress materials or *viscoplastic fluids* are ubiquitous in nature and they are encountered daily in a variety of forms: foods (mayonnaise, molten chocolate, mustard, ketchup), cosmetic products (shaving foam, tooth paste, hair gel, shampoos, hand and face creams), drilling muds, cements, volcanic lava, molten metals etc. A particular class of yield stress materials is the *physical gel*. Due to their large water content, the physical gels are compatible with biological tissues which makes them excellent candidates for various biomedical applications: targeted drug delivery [1, 2], contact lenses, noninvasive intervertebral disc repair [3] and tissue engineering [4].

From a mechanical perspective, such materials behave as solids if the stresses applied onto them are smaller than a threshold value σ_y generally referred to as the "yield stress" and as fluids otherwise. At a macroscopic scale, this behavior is generally illustrated by the Herschel-Bulkley law [5, 6], $\sigma = \sigma_y + K\dot{\gamma}^N$. Here $\dot{\gamma}$ is the rate of shear, i.e., the rate at which the material is being deformed, σ is the externally applied stress to cause this deformation, K is a so-called consistency parameter that sets the viscosity scale in the flowing state and N is the power law index which characterizes the degree of shear thinning of the viscosity beyond the yield point. In the particular case of a Newtonian behavior beyond the yield point with $N = 1$, this model reduces to the Bingham model [7].

In spite of its wide use by rheologists, fluid dynamicists and engineers, the Herschel-Bulkley model (and its regularized variants, e.g. Papanastasiou [8]) is in fact applicable only for a limited number of yield stress materials, sufficiently far from the solid-fluid transition, i.e. when $\sigma > \sigma_y$, and in the conditions of a steady state forcing, i.e. when a constant external stress σ is applied over a long period of time. Thixotropy, which may be loosely understood as a time dependence of the rheological parameters which results from a competition between destruction and rejuvenation of the soft material units subjected to stress, is a major reason for the departure from this simple yielding scenario [9]. It has been shown recently that a clear departure from the Herschel-Bulkley behavior can be observed even for non-thixotropic yield stress fluids such as the Carbopol gels particularly during unsteady flows taking place around the yield point [10, 11].

To overcome these difficulties, several phenomenological macroscopic models have been proposed [12, 13, 14, 15, 16, 10, 17]. The common feature of these models is the quantity $\overline{a}(t)$, the volume fraction of the unyielded material at time t whose time evolution is directly related to the applied stress. Thus, as the applied stress is increased, $\overline{a}(t)$ varies smoothly from 1 to 0 and the combined solid and fluid rheological responses are weighted accordingly into a constitutive relation. As opposed to the Bingham and the Herschel-Bulkley models which predict an abrupt and discontinuous solid-fluid transition when $\overline{a}$ jumps from 1 to 0 at a well defined value of the applied stress, say, $\sigma = \sigma_y$, such approaches which directly account for the evolution of $\overline{a}(t)$ are able to describe several features observed in experiments, such as, (i) a smooth (gradual) solid-fluid transition (ii) the irreversibility of the deformation states upon increasing/decreasing applied stresses that is implied by

an observed hysteresis and (iii) a clear dependence of the yielding/gelating scenario, as reflected by the area of the hysteresis, on the degree of the steadiness of the external forcing, i.e. how fast is the external stress varied about the solid-fluid transition [10, 11].

Though able to model sufficiently complex rheological data (ranging from controlled stress/strain unsteady flow ramps, creep tests and oscillatory tests in a wide range of frequencies and amplitudes), such phenomenological macroscopic models do have a number of limitations. First, they typically involve a rather large number of parameters which are not directly and easily measurable and can be obtained only by fitting the experimental data. Second, such models are not inherently validated from a thermodynamical standpoint — the second law of thermodynamics is not guaranteed to be held — and such a validation is not always straightforward as it requires the derivation of a thermodynamic potential [18, 19].

As the macroscopic yield stress behavior originates from the presence of a "soft" microstructure which can locally sustain only a finite stress prior to its breakdown, an alternative way of assessing the dynamics of the yielding process is to focus on the evolution of the micro-structural soft material units or clumps of particles as the external stress is gradually increased past the solid-fluid transition and next to assess the macroscopic scale behavior from the perspective of statistical mechanics.

There exist only few theoretical and/or experimental studies focusing on the microscopic scale description of the macroscopic yielding (a deformative transformation of solid to fluid under an increasing stress regime) *and* the macroscopic gelation (a constitutive transformation of liquid to solid under a decreasing stress regime) of physical gels. This sets the main scope of the present contribution.

A thermodynamic approach for the deformation of a physical gel has been recently proposed by An and coworkers [20]. By using a mean field approach, they construct a free energy functional and describe the microscopic scale dynamics of the gel network as a function of the applied stress in terms of the monomer volume fraction and an internal connectivity tensor characterizing the gel network. As the free energy functional they propose accounts for the elastic energy, the mixing energy and the bond energy, the approach of An and coworkers is quite general and is expected to be applicable to a broad class of physical gels and chemical gels with a fixed number of monomers per cross-link.

de Bruyn [21] has modelled the restricted diffusion of small tracer particles in heterogeneous media by performing Monte Carlo simulations in a site-percolation model. His simulations reveal a transition from a viscous to an elastic behavior at a site-filling probability that is different from that corresponding to the percolation transition. He explains this finding by the confinement of the tracers in the spatially heterogeneous medium which makes the general Stokes-Einstein relation inapplicable in this case. A partial agreement between the results of the simulation and experimental results is found, [22, 23].

We propose in the following a microscopic model for the yielding or gelation, corresponding to $\overline{a}$ approaching 0 or 1 respectively, of a physical gel using an essentially bi-parametric family of a correlated site percolation that is inspired by the two dimensional Ising model for the $+1$ or -1 magnetization of a ferromagnet [24, 25]. Our model builds on the analogy between the local agglomerative interactions in terms of assembly/disassembly of neighboring gel particles in a microscopic gel network — see [26, (2.5,2.6,5.9,5.9.1,5.9.1.1,8.1.4)] and [27] for standardized nomenclature — subjected to an external stress and the local ferromagnetic interactions in terms of spin up $(+1)$ / spin down (-1) of neighboring particles in a microscopic ferromagnetic network subjected to an external magnetic field.

Our thermodynamically consistent microscopic model with only two parameters that reflect the rheological properties of the gel and only two energy-determining configuration statistics — the number of gelled particles and the number of gelled pairs of neighboring particles — is able to capture the macroscopic behaviors of yielding and gelation for any stress regime given as a function of time, including hysteretic effects, if any. Our approach is fundamentally probabilistic and formalizes Gibbs fields as time-homogeneous and time-inhomogeneous Markov chains over the state space of all microscopic configurations. We not only provide simulation algorithms to gain insights but also derive an approximating nonlinear ordinary differential equation for $\overline{a}(t)$, the expected volume fraction of the unyielded material at a rescaled time t, which we show to be a robust qualitative determinant of the probabilistic dynamics of the system.

The paper is organized as follows. The mathematical formulation of the model and the simulation algorithm are presented in Sec. 2. A differential equation approximating the expected solid fraction of the material in the Gibbs model is derived and analyzed in Sec. 3. The results of the simulations according to the microscopic model and the expected trajectories from the approximating differential equation are presented in Sec. 4. The paper concludes in Sec. 5 with a discussion of the main findings and their possible implications and extensions.

2. Model

Let us model an idealized yield stress material or viscoplastic fluid as a network of particles in an appropriate solvent that are capable of assembling by "forming bonds" or disassembling by "breaking bonds" with their neighbors. We investigate the model when the network of particles is the regular graph given by the toroidal two-dimensional square lattice. Let the set of nodes or sites be

$$\mathbb{S}_n = \{1, 2, \ldots, n\}^2 = \{(1,1), (1,2), \ldots, \ldots, (n,n)\} \ .$$

Let $N_s = \{r : \|\overline{(r-s)}_n\| = 1\}$ denote the set of four nearest neighboring sites of a given site $s \in \mathbb{S}_n$, where $\overline{(r-s)}_n$ denotes coordinate-wise subtraction modulo n and $\|\cdot\|$ denotes the Euclidean distance. Then the set of edges between pairs of sites is

$$\mathbb{E}_n = \bigcup_{s \in \mathbb{S}_n} \{\langle s, r\rangle : r \in N_s\} \subset \mathbb{S}_n^2 \ .$$

Let $|A|$ denote the size of the set A. Note that $|\mathbb{S}_n| = n^2$ and $|\mathbb{E}_n| = 2n^2$. Each site $s \in \mathbb{S}_n$ can be thought to represent a mi-

croscopic *clump* of particles in a particular region of the material and each edge $\langle s, r\rangle \in \mathbb{E}_n$ represents a potential *connection* between neighboring clumps at sites s and r. At the finest resolution of the model, each site can be a monomer molecule in the material and each edge can represent a potential bond between neighboring molecules. Let $x_s \in \Lambda = \{0, 1\}$ denote the phase at site s. Phase 0 corresponds to being *yielded* or *ungelled* and phase 1 corresponds to being *unyielded* or *gelled*. The phase at a site directly affects its *connectability* with its neighboring sites. We assume that only two gelled sites can be connected with one another. Thus, the connectivity between sites s and r is given by

$$y_{\langle s,r\rangle} = \begin{cases} 1 & \text{if } r \in N_s \text{ and } x_r x_s = 1 \\ 0 & \text{otherwise.} \end{cases} \tag{1}$$

In other words, we say that sites s and r are *connected*, i.e., $y_{\langle s,r\rangle} = 1$, if and only if $x_s = x_r = 1$ and s and r are neighbors. Otherwise, we say s and r are *unconnected*, i.e., $y_{\langle s,r\rangle} = 0$. Since the phase of sites determine their connectedness, we refer to sites in phase 1 as *connectable* and those in phase 0 as *unconnectable*. Thus, every site configuration $x \in \mathbb{X}_n := \Lambda^{\mathbb{S}_n}$ has an associated *edge configuration* $y \in \mathbb{Y}_n := \Lambda^{\mathbb{E}_n}$ which characterizes the connectivity information between all pairs of neighboring sites. We use X to denote a *random site configuration* and $Y = Y(X)$ to denote the associated *random edge configuration*. Two extreme site configurations are $\mathbf{1} := \{x_s = 1 : s \in \mathbb{S}_n\} \in \mathbb{X}_n$, with all sites gelled, and $\mathbf{0} := \{x_s = 0 : s \in \mathbb{S}_n\} \in \mathbb{X}_n$, with all sites ungelled. Their corresponding extreme edge configurations are $\mathbf{1} := \{y_{\langle s,r\rangle} = 1 : \langle s, r\rangle \in \mathbb{E}_n\} \in \mathbb{Y}_n$, with all neighboring pairs of sites connected and thus making the material to be in a fully solid state, and $\mathbf{0} := \{y_{\langle s,r\rangle} = 0 : \langle s, r\rangle \in \mathbb{E}_n\} \in \mathbb{Y}_n$, with all neighboring pairs of sites unconnected and thus making the material to be in a fully fluid state, respectively. Note that $Y(x) : \mathbb{X}_n \to \mathbb{Y}_n$ is neither injective nor surjective.

Let $\mathcal{E}(x)$ be the energy of a site configuration x, k be the Boltzmann constant and T be the thermal temperature. Then the probability distribution of interest on the site configuration space $\mathbb{X}_n$ is

$$\pi(x) = \frac{1}{Z_{kT}} \exp\left(-\frac{1}{kT}\mathcal{E}(x)\right) \ ,$$

where Z_{kT} is the normalizing constant or partition function

$$Z_{kT} = \sum_{x\in\mathbb{X}_n} \exp\left(-\frac{1}{kT}\mathcal{E}(x)\right) \ .$$

By $X \sim \pi$, we mean that the random site configuration X has probability distribution π, i.e.,

$$\Pr(X = x) = \begin{cases} \pi(x) & \text{if } x \in \mathbb{X}_n \\ 0 & \text{otherwise} \ . \end{cases}$$

Next we show that π is a Gibbs distribution by expressing the energy in terms of a potential function describing local interactions. Due to $\{N_s : s \in \mathbb{S}_n\}$, the neighborhood system, we have only singleton and doubleton cliques. Therefore, the Gibbs potential over the two types of cliques are:

$$V_{\{s\}}(x) = (\sigma - \alpha)x_s = \begin{cases} 0 & \text{if } x_s = 0 \\ \sigma - \alpha & \text{if } x_s = 1 \ , \end{cases}$$

and

$$V_{\langle s,r\rangle}(x) = -\beta x_s x_r = \begin{cases} 0 & \text{if } (x_s, x_r) = (0, 0) \\ 0 & \text{if } (x_s, x_r) = (1, 0) \\ 0 & \text{if } (x_s, x_r) = (0, 1) \\ -\beta & \text{if } (x_s, x_r) = (1, 1) \ , \end{cases}$$

where $\{s\}$ is the singleton clique, $\langle s, r\rangle$ is the doubleton clique with $r \in N_s$, $\sigma \geq 0$ is the external stress applied, $\alpha \geq 0$ is the *site-specific threshold*, and $\beta \in (-\infty, \infty)$ is the *interaction constant* between neighboring sites. The parameters α and β can be thought to reflect fundamental rheological properties of the material under study.

The energy function corresponding to this potential is therefore

$$\begin{aligned} \mathcal{E}(x) &= \sum_C V_C(x) \\ &= \sum_{s\in\mathbb{S}_n} V_{\{s\}}(x) + \sum_{\langle s,r\rangle\in\mathbb{E}_n} V_{\langle s,r\rangle}(x) \\ &= \left(-\beta \sum_{\langle s,r\rangle\in\mathbb{E}_n} x_s x_r + (\sigma - \alpha) \sum_{s\in\mathbb{S}_n} x_s\right) \ . \end{aligned}$$

Since $\mathcal{E}(x)$, the energy of a configuration x, only depends on β and the difference $(\sigma - \alpha)$, we can define this difference as the parameter $\tilde{\sigma} := \sigma - \alpha \geq -\alpha$ in order to reparametrize

$$\mathcal{E}(x) = \left(-\beta \sum_{\langle s,r\rangle\in\mathbb{E}_n} x_s x_r + \tilde{\sigma} \sum_{s\in\mathbb{S}_n} x_s\right) \ ,$$

through $(\tilde{\sigma}, \beta) \in [-\alpha, \infty) \times (-\infty, \infty)$.

Let the expectation of a function $g : \mathbb{X}_n \to \mathbb{R}$, with respect to π, be

$$\mathbf{E}_\pi(g) := \sum_{x\in\mathbb{X}_n} g(x)\pi(x)$$

then the *internal energy* of the system is

$$\mathcal{U} = \mathbf{E}_\pi(\mathcal{E}) = \sum_{x\in\mathbb{X}_n} \mathcal{E}(x)\pi(x) \ ,$$

and the *free energy* of the system is

$$\mathcal{F} = -kT \ln(Z_{kT}) \ .$$

Our model satisfies the standard thermodynamic equality:

$$\begin{aligned} &-T^2 \frac{\partial}{\partial T}\left(\frac{\mathcal{F}}{T}\right) = -T^2 \frac{\partial}{\partial T}\left(\frac{-kT\ln(Z_{kT})}{T}\right) = kT^2 \frac{\partial}{\partial T}\left(\ln(Z_{kT})\right) \\ &= kT^2 \frac{1}{Z_{kT}} \frac{\partial}{\partial T}\left(Z_{kT}\right) = kT^2 \frac{1}{Z_{kT}} \frac{\partial}{\partial T}\left(\sum_{x\in\mathbb{X}_n} \exp\left(-\frac{1}{kT}\mathcal{E}(x)\right)\right) \\ &= kT^2 \frac{1}{Z_{kT}} \left(\sum_{x\in\mathbb{X}_n} \exp\left(-\frac{1}{kT}\mathcal{E}(x)\right) \frac{\mathcal{E}(x)}{kT^2}\right) = \sum_{x\in\mathbb{X}_n} \mathcal{E}(x)\pi(x) \\ &= \mathcal{U} \ . \end{aligned}$$

We sometimes emphasize the dependence of the energy and the corresponding distribution upon α, β and σ by subscripting as follows:

$$\mathcal{E}(x) = \mathcal{E}_{\alpha,\beta,\sigma}(x) \quad \text{and} \quad \pi(x) = \pi_{\alpha,\beta,\sigma}(x) \ .$$

2.1. Local Specification

Let the number of neighbors of site s that are in phase 1 be $x_{N_s} := \sum_{r\in N_s} x_r$. Then, $\mathcal{E}_s(x)$, the *local energy* at site s of configuration x, is obtained by summing the Gibbs potential $V_C(x)$ over all $C \ni s$, i.e., over cliques C containing site s, as follows

$$\begin{aligned}
\mathcal{E}_s(x) &= \sum_{C\ni s} V_C(x) = V_{\{s\}}(x) + \sum_{r\in N_s} V_{\langle s,r\rangle}(x) \\
&= (\sigma-\alpha)x_s - \beta \sum_{r\in N_s} x_s x_r \\
&= x_s\left((\sigma-\alpha) - \beta\sum_{r\in N_s} x_r\right) \\
&= x_s\left((\sigma-\alpha) - \beta x_{N_s}\right) \ .
\end{aligned}$$

Let $(\lambda, x(\mathbb{S}\setminus s))$ denote the configuration that is in phase λ at s and identical to x everywhere else. Then the *local specification* is

$$\begin{aligned}
\pi_s(x) &= \frac{\exp(-\frac{1}{kT}\mathcal{E}_s(x))}{\sum_{\lambda\in\Lambda}\exp(-\frac{1}{kT}\mathcal{E}_s(\lambda, x(\mathbb{S}\setminus s)))} \\
&= \begin{cases} \frac{\theta}{1+\theta} & \text{if } x_s = 0 \\ \frac{1}{1+\theta} & \text{if } x_s = 1 \end{cases} \ , \qquad (2)
\end{aligned}$$

where

$$\theta = \theta(s,\alpha,\beta,\sigma) = \exp\left(-\frac{1}{kT}\left(\beta x_{N_s} - (\sigma-\alpha)\right)\right) \ . \qquad (3)$$

In this work we focus on the effect of varying external stress σ at a constant ambient temperature, and therefore without loss of generality, we take $kT = 1$ and work with $\pi(x) = Z_1^{-1}\exp(-\mathcal{E}(x))$.

2.2. Markov chain on configuration space

We can think of our model as an $\mathbb{X}_n$-valued Markov chain $\{X(m)\}_{m=0}^{\infty}$, where $X(m) = (X_s(m), s\in\mathbb{S}_n)$ and $X_s(m)\in\Lambda$, in discrete time $m\in\mathbb{Z}_+ := \{0,1,2,\ldots\}$. Let the initial condition, $X(0) = x(0)$, be given by the initial distribution $\delta_{x(0)}$ over $\mathbb{X}_n$ that is entirely concentrated at state $x(0)$. Then the conditional probability of the Markov chain at time-step m, given that it starts at time 0 in state $x(0)$, is

$$\Pr\{X(m)\,|\,X(0) = x(0)\} = \delta_{x(0)}\left(P_{\alpha,\beta,\sigma}\right)^m \ , \qquad (4)$$

where, the $|\mathbb{X}_n|\times|\mathbb{X}_n|$ transition probability matrix $P_{\alpha,\beta,\sigma}$ over any pair of configurations $(x,x')\in\mathbb{X}_n\times\mathbb{X}_n$ is

$$P_{\alpha,\beta,\sigma}(x,x') = \begin{cases} \frac{1}{n^2}\frac{1}{1+\theta} & \text{if } \|x-x'\| = 1, 0 = x_s \neq x'_s = 1 \\ \frac{1}{n^2}\frac{\theta}{1+\theta} & \text{if } \|x-x'\| = 1, 1 = x_s \neq x'_s = 0 \\ \frac{1}{n^2}\frac{1}{1+\theta} & \text{if } \|x-x'\| = 0, 1 = x_s = x'_s = 1 \\ \frac{1}{n^2}\frac{\theta}{1+\theta} & \text{if } \|x-x'\| = 0, 0 = x_s = x'_s = 0 \\ 0 & \text{otherwise} \ . \end{cases} \qquad (5)$$

and $\theta = \theta(s,\alpha,\beta,\sigma)$, is indeed a function of the site s and the three parameters: α, β and σ. By $\|x-x'\| = 1$ we mean that the configurations x and x' differ at exactly site s, i.e., $x_s \neq x'_s$. Similarly, by $\|x-x'\| = 0$ we mean that the two configurations are identical, i.e., $x = x'$ or $x_s = x'_s$ at every site $s\in\mathbb{S}_n$. We can think of our Markov chain evolving according to the following probabilistic rules based on (2) and (3):

- given the current configuration x, we first choose one of the n^2 sites in $\mathbb{S}_n$ uniformly at random with probability n^{-2},
- denote this chosen site by s and let the number of bondable neighbors of s be $i = N_s(x)\in\{0,1,2,3,4\}$, and
- finally change the phase at s to 1, i.e., set $x_s = 1$ with probability

$$p_i := (1+\theta)^{-1} = (1+\theta(s,\alpha,\beta,\sigma))^{-1} = 1/(1+e^{(\sigma-\alpha-i\beta)}) \qquad (6)$$

and set $x_s = 0$ with probability $1-p_i$.

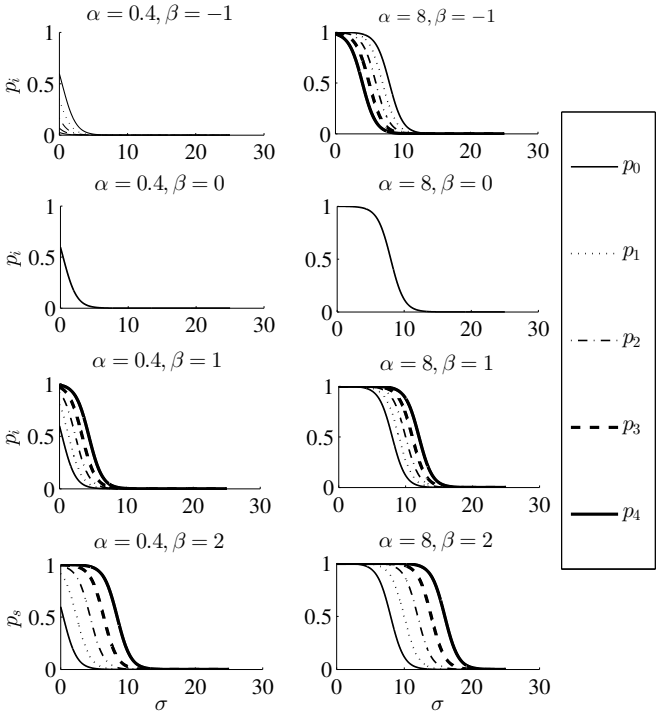

Figure 1: Plots of p_i, the probability that site s with $i = x_{N_s}$ neighbors in phase 1, is also in phase 1, as a function of external stress σ for different values of α, β. From the plots it is clear that α is a location parameter while β controls the scale of the relative difference between p_i's.

We emphasize the dependence of p_i on the parameters α, β and σ by $p_i(\alpha,\beta,\sigma)$. This is plotted in Fig. 1 for different parameter values. Just as in the Ising model, our model can be classified into three behavioral regimes depending on the sign of the interaction parameter β. When the interaction parameter $\beta > 0$ the model is said to have *agglomerative interactions* analogous to the to the *ferromagnetic* interactions of the Ising

model [28, Sec. C.V.4, p.133] whereby the probability of a site being in phase 1 increases with the number of its neighboring sites also being in phase 1, i.e., if $\beta > 0$ then

$$0 < p_0 < p_1 < p_2 < p_3 < p_4 < 1 \ .$$

When $\beta = 0$ the model is said to be *non-interactive* since the probability of a site being in phase 1 is independent of the phase of the neighboring sites and identically p at each site, i.e.,

$$0 < p = p_0 = p_1 = p_2 = p_3 = p_4 = 1/\left(1 + e^{\sigma-\alpha}\right) < 1.$$

When $\beta < 0$, our model captures the *anti-agglomerative* interactions that are analogous to the *anti-ferromagnetic* interactions of the Ising model [28, Sec. C.V.4, p.133] since the probability of a site being in phase 1 decreases with the number of its neighboring sites also being in phase 1, i.e., if $\beta < 0$ then

$$1 > p_0 > p_1 > p_2 > p_3 > p_4 > 0 \ .$$

Note that our transition probabilities allow *self-transitions*, i.e., there is a positive probability that we will go from a configuration x to itself. Although we think of $\{X(m)\}_{m=0}^{\infty}$ on the state space of all configurations $\mathbb{X}_n$ as a discrete-time Markov chain, with transition probability matrix $P_{\alpha,\beta,\sigma}$ in (5), we can easily add exponentially distributed holding times with rate 1 at each configuration and use (5) to choose a possibly new configuration and thereby obtain a continuous time Markov chain $\{X(t)\}_{t\geq 0}$ in the usual way from $\{X(m)\}_{m=0}^{\infty}$. This Markov chain over $\mathbb{X}_n$ is nothing but our Gibbs field (or Markov random field) model [29, see for e.g. Ch. 7].

If the external stress varies as a function of discrete time-blocks of length $\underline{h} = \lfloor hn^2 \rfloor$ and given by the function $\sigma(m)$ for each time-block $m = 0, 1, \ldots, M$ then we have the time-inhomogeneous Markov chain $\{X(k)\}_{k=0}^{M\underline{h}}$ with the transition probability matrix at time k given by

$$P(k) = P_{\alpha,\beta,\sigma(\lfloor k/\underline{h} \rfloor)} \ , \tag{7}$$

and the k-step configuration probability, with $k < M\underline{h}$ under initial distribution $\delta_{x(0)}$, given by

$$\begin{aligned}&\Pr\{\, X(k) = x(k) \,|\, X(0) = x(0) \,\} \\ &\qquad = \delta_{x(0)} \left(\prod_{m=0}^{\lfloor k/\underline{h} \rfloor} \left(P_{\alpha,\beta,\sigma(m)} \right)^{\underline{h}} \right) \left(P_{\alpha,\beta,\sigma(\lfloor k/\underline{h} \rfloor + 1)} \right)^{\overline{(k)}_{\underline{h}}} \ . \end{aligned} \tag{8}$$

As before, $\overline{(k)}_{\underline{h}}$ is k modulo $\underline{h}$.

2.3. Gibbs sampling

We can use the local specification to obtain the Gibbs sampler, a Monte Carlo Markov chain (MCMC), to simulate from $\{X(m)\}$. Let h denote the average number of hits per site. Thus, $\lfloor h|\mathbb{S}_n| \rfloor = \lfloor hn^2 \rfloor$ gives the number of hits on all n^2 sites in $\mathbb{S}_n$ chosen uniformly at random. Given h and the parameters determining the local specification, i.e., α, β and σ, `GibbsSample`$(x(0), \alpha, \beta, \sigma, h)$ in Algorithm 1 of Appendix A produces a sample path of configurations

$$(\, x(0), x(1), \ldots, x(m) \,) \in x(0) \times \left(\overset{m}{\underset{i=1}{\times}} \mathbb{X}_n \right) = x(0) \times \mathbb{X}_n^m$$

from the Markov chain $\{X(k)\}_{k=0}^{m}$ given by (4) and (5) and initialized at $x(0)$ as it undergoes $m = \lfloor hn^2 \rfloor$ transitions in $\mathbb{X}_n$.

If we are interested in simulating configurations with stationary distribution $\pi_{\alpha,\beta,\sigma}$, then for large $m = \lfloor hn^2 \rfloor$, the m-step probabilities, $\Pr\{\, X(m) \,|\, X(0) = x(0) \,\}$, by construction will approximate samples from $\pi_{\alpha,\beta,\sigma}$ [29, see for e.g. Ch. 7, Sec. 6], i.e.,

$$\lim_{m\to\infty} d_{TV}\left(\Pr\{\, X(m) \,|\, X(0) = x(0) \,\}, \pi_{\alpha,\beta,\sigma} \right) = 0 \ .$$

Here, $d_{TV}(\varpi, \pi) = 2^{-1} \sum_{x\in\mathbb{X}_n} |\varpi(x) - \pi(x)|$ is the total variation distance between two distributions ϖ and π over $\mathbb{X}_n$.

We can just as easily produce samples from the time-inhomogeneous Markov chain $\{X(k)\}_{k=0}^{M\underline{h}}$ given by (7) and (8) according to Algorithm 2 of Appendix A [30, see for eg. pp. 21-22].

2.4. Sufficient Configuration Statistics for Energy

Two informative singleton clique statistics of a configuration $x(m)$ at time m are the number and fraction of gelled sites given respectively by

$$a(x) := \sum_{s\in\mathbb{S}_n} x_s \quad \text{and} \quad \overline{a}(x) := |\mathbb{S}_n|^{-1} a(x) = \frac{a(x)}{n^2} \ .$$

Similarly, two informative doubleton clique statistics of a configuration x are the number and fraction of connected pairs of neighboring sites given respectively by

$$\begin{aligned} b(x) &:= \sum_{\langle s,t\rangle\in\mathbb{E}_n} y_{\langle s,r\rangle} = \sum_{\langle s,r\rangle\in\mathbb{E}_n} x_r x_s \quad \text{and} \\ \overline{b}(x) &:= |\mathbb{E}_n|^{-1} b(x) = \frac{b(x)}{2n^2} \ . \end{aligned}$$

When the configuration is a function of time m and given by $x(m)$, then the corresponding configuration statistics are also functions of time and are given by: $a(m) = a(x(m))$, $\overline{a}(m) = \overline{a}(x(m))$, $b(m) = b(x(m))$ and $\overline{b}(m) = \overline{b}(x(m))$. The energy of a configuration x can be succinctly expressed in terms of $\overline{a}(x)$ and $\overline{b}(x)$ as

$$\mathcal{E}(x) = -\beta b(x) + (\sigma - \alpha) a(x) = -\beta 2n^2 \overline{b}(x) + (\sigma - \alpha) n^2 \overline{a}(x) \ ,$$

and therefore

$$\mathcal{E}(x) \propto -2\beta\overline{b}(x) + (\sigma - \alpha)\overline{a}(x) = -2\beta\overline{b}(x) + \tilde{\sigma}\overline{a}(x) \ , \tag{9}$$

where $\beta \in (-\infty, \infty)$ and $\tilde{\sigma} = \sigma - \alpha \geq -\alpha$ for a given $\alpha \geq 0$. Since the energy of a configuration x, given n, only depends on its $\overline{a}(x)$ and $\overline{b}(x)$, we can easily visualize any sample path $(\, x(0), \ldots, x(m) \,) \in \mathbb{X}_n^{m+1}$ in configuration space that is outputted by either Algorithm 1 or Algorithm 2 as the following sequence of $(m+1)$ ordered pairs in the unit square:

$$\left(\left(\overline{a}(x(0)), \overline{b}(x(0)) \right), \ldots, \left(\overline{a}(x(m)), \overline{b}(x(m)) \right) \right) \in \left([0,1]^2 \right)^{m+1} \ .$$

Finally, we reserve upper-case letters for random variables. Thus, $A(X)$, $\overline{A}(X)$, $B(X)$ and $\overline{B}(X)$ are the statistics of the random configuration X. And the notation naturally extends to $A(m)$, $\overline{A}(m)$, $B(m)$ and $\overline{B}(m)$ when $X(m)$ is a random configuration at time m.

2.5. Other Configuration Statistics

The macroscopic behavior of a configuration x can be described by other statistics of x. We can obtain the connectivity information in the site configuration x through y, its edge configuration, according to (1). By representing the connectivity in y and/or x as the adjacency matrix of the graph whose vertices are $\mathbb{S}_n$, we can obtain various graph statistics, including (i) $C_x = \left\{C_x^{(1)}, C_x^{(2)}, \ldots, C_x^{(n_y)}\right\}$, a partition of $\mathbb{S}_n$ that gives the set of connected components of x, (ii) $C_x^{(*)} = \text{argmax}_{C_x^{(i)} \in C_x} |C_x^{(i)}|$, the first largest connected component, (iii) $|C_x^{(*)}|/n^2$, the size of the first largest connected component per site, and (iv) $F_x^{(*)}$, the fraction of the rows of $\mathbb{S}_n$ that are permeated (from top to bottom) by $C_x^{(*)}$.

2.6. Relations to Existing Models

Among the ten models discussed in a detailed review article [28, Sec. C.V.] and the classical models of interacting particle systems [31] our Gibbs field model — a parametric family of spin systems or Markov random fields — is most closely related to the following three models.

2.6.1. Site Percolation Model

In a site percolation model, a randomly chosen fraction p of sites are set to be in phase 1; these sites represent gelled regions of the material while the remaining sites in phase 0 represent ungelled or fluid regions. Our non-interactive model ($\beta = 0$) in the presence of a constant external stress ($\sigma \in [0, \infty)$) is the site percolation model over $\mathbb{S}_n$ with site-filling probability $p = (1 + e^{\sigma-\alpha})^{-1}$. In the absence of external stress with $\sigma = 0$ we have the site percolation model with site-filling probability $p = (1 + e^{-\alpha})^{-1}$. As p increases from 0, the size of the largest connected region of gelled sites grows and at a critical probability $p = p_c \cong 0.5927$ (for large n) a *percolation cluster* that spans the entire lattice $\mathbb{S}_n$ appears when $F_x^{(*)} = 1$ for site configuration x. We note that the value of p_c for site percolation, unlike for bond percolation where we only track the presence or absence of bonds between adjacent sites, is not yet known exactly (although various inequalities, identities and asymptotically consistent point estimates are known [32, for e.g. see Secs. 5.3,6.1,6.4]). Finally, site percolation is more general than bond percolation and can, at least in principle, be used to model richer phenomena. Our interpretation of the site configuration where each site is either bondable or unbondable and its associated edge configuration where only two neighboring bondable sites form a bond, is not as strict as the interpretation in the *random-site percolation* model of [28, Sec. C.V.1, p.130] that "bonds between sites always exist". In our interpretation, bonds between sites only exist if two neighboring sites are bondable, i.e., they are both in phase 1.

2.6.2. Voter Model

Our model is closely related to the embedded discrete time Markov chain in the classical *voter process* [31, Ch. 5] of probability theory, whereby at each site a voter casts one of two votes (0 or 1) by copying the vote of one of its randomly chosen four nearest neighbors in $\mathbb{S}_n$. If the voter at each site chooses one of its four neighbors uniformly at random, then the voter model corresponds to our model with

$$p_0 = 0, p_1 = 1/4, p_2 = 1/2, p_3 = 3/4, p_4 = 1 \ . \tag{10}$$

More generally, one can allow $0 \le p_0 \le p_1 \le p_2 \le p_3 \le p_4 \le 1$ to recover a corresponding voter process that is possibly influenced by the neighboring votes. Thus, in the square lattice $\mathbb{S}_n$ with four nearest neighbors, every point $(p_0, p_1, \ldots, p_4)$ in $\triangle^4$, the unit 4-simplex containing the set of all probability mass functions over $\{0, 1, 2, 3, 4\}$, defines a voter process. We can think of $\triangle^4$-indexed voter process as a discrete non-parametric extension of the classical parameter-free voter process of (10).

Finally, for a fixed $\beta \in (-\infty, \infty)$ and a fixed $\tilde{\sigma} = \sigma - \alpha \ge -\alpha$, our model can be thought of as a $(\tilde{\sigma}, \beta)$-parametric specification of the discrete time voter model (which can be extended in the usual way to continuous time by introducing independent exponential holding times with rate 1). For example, with $kT = 1$, $\beta = \ln(3)$ and $\tilde{\sigma} = \sigma - \alpha = 2\ln(3)$, we can get the parameters of our model to be close to that of the classical voter model in (10) but with

$$p_0 = 1/10, p_1 = 1/4, p_2 = 1/2, p_3 = 3/4, p_4 = 9/10 \ .$$

We note that the classical voter model allows for extreme probabilities with $p_0 = 0$ and $p_1 = 1$ and this turns the two extreme site configurations with all 0's and all 1's, i.e., $\mathbf{0}$ and $\mathbf{1}$, into absorbing states. However, in our model the probabilities are non-extreme, i.e., $0 < p_0 < 1$ and $0 < p_1 < 1$, and thus our Markov chain is irreducible and aperiodic (due to self-transitions) on the large but finite configuration space $\mathbb{X}_n$. Moreover, when $\beta < 0$, the corresponding model with $1 > p_0 > p_1 > p_2 > p_3 > p_4 > 0$ (see top row of Fig. 1) is akin to the *anti-voter model* [31, p. 162]. Finally, our set of sites $\mathbb{S}_n$ is finite and we take the limit as $n \to \infty$ in the sequel, but the set of sites in the classical voter model is the countably infinite $\mathbb{Z}^2 = \{\ldots, -2, -1, 0, 1, 2, \ldots\}^2$.

2.6.3. Correlated Site Percolation Model

Our model with $\beta \neq 0$ allows for correlation between the phases due to nearest-neighbor interactions. This is nearly the same as the *correlated site percolation* model of [28, Sec. C.V.3, p.131] inspired by the classical Ising model for ferro-magnetism. One crucial difference is that we have thermal temperature as well as external stress in our parametrization and focus on the system behavior under variable external stress and constant temperature for a given pair of rheological parameters α and β. Our model is also inspired by the Ising model with phases given by $\{0, 1\}$ for the bondability of sites as opposed to $\{-1, +1\}$ for the ferromagnetic spins.

3. An Approximating Nonlinear Dynamical System

Here we derive a nonlinear first-order differential equation to asymptotically approximate $\mathbf{E}(\overline{A}(t))$, the expected fraction of sites in the solid phase, in continuous time t that is measured in units of n^2 discrete time-steps as the number of sites $n^2 \to \infty$,

under a fixed externally applied stress σ and fixed rheological parameters α and β.

First consider the discrete-time Markov chain $\{X(m)\}_{m=0}^{\infty}$ of (4) and (5) and recall that $X(m)$ is the random site configuration of the chain at discrete time m and $A(m) = \sum_s X_s(m)$ is the number of sites that are in phase 1. We will derive the approximation first for the case when $\beta = 0$ in (5) and then for the general setting of $\beta \neq 0$.

3.1. Non-interactive case with $\beta = 0$

If $\beta = 0$ then the probability of the phase in site s at the next time-step is independent of the current configuration, i.e.,

$$\begin{aligned}
&\Pr\{X_s(m+1) = x_s(m+1) \,|\, X(m) = x(m)\} \\
&\quad = \Pr\{X_s(m+1) = x_s(m+1)\} \\
&\quad = \begin{cases} p = (1+e^{\sigma-\alpha})^{-1} & \text{if } x_s(m+1) = 1 \\ 1-p = 1-(1+e^{\sigma-\alpha})^{-1} & \text{if } x_s(m+1) = 0 \\ 0 & \text{if } x_s(m+1) \notin \{0,1\} \end{cases} .
\end{aligned}$$

Therefore, the probability that the total number of sites in phase 1 increases by 1 in one time-step is obtained by adding the probability of a transition from phase 0 to phase 1 over every uniformly chosen site s as follows:

$$\begin{aligned}
&\Pr\{A(m+1) = a(m)+1 \,|\, A(m) = a(m)\} \\
&= \sum_{s\in\mathbb{S}_n} \Pr\{X_s(m+1) = 1, X_s(m) = 0, S = s \,|\, A(m) = a(m)\} \\
&= \sum_{s\in\mathbb{S}_n} \underbrace{\Pr\{X_s(m+1) = 1 \,|\, X_s(m) = 0, S = s, A(m) = a(m)\}}_{p} \\
&\qquad\qquad \times \underbrace{\Pr\{X_s(m) = 0 \,|\, S = s, A(m) = a(m)\}}_{(n^2-a(m))/n^2} \\
&\qquad\qquad\qquad \times \underbrace{\Pr\{S = s \,|\, A(m) = a(m)\}}_{1/n^2} \\
&\qquad\qquad\qquad = \sum_{s\in\mathbb{S}_n} p\left(1-\frac{a(m)}{n^2}\right)\frac{1}{n^2} = p\,(1-\overline{a}(m)) .
\end{aligned}$$

Dividing both sides of the equality that defines the above event by n^2 we get

$$\begin{aligned}
&\Pr\left\{A(m+1)/n^2 = a(m)/n^2 + 1/n^2 \,\middle|\, A(m)/n^2 = a(m)/n^2\right\} \\
&= \Pr\left\{\overline{A}(m+1) = \overline{a}(m) + 1/n^2 \,\middle|\, \overline{A}(m) = \overline{a}(m)\right\} = p\,(1-\overline{a}(m)) .
\end{aligned}$$

By an analogous argument we can obtain the probabilities for the remaining two possibilities

$$\begin{aligned}
\Pr\left\{\overline{A}(m+1) = \overline{a}(m) - 1/n^2 \,\middle|\, \overline{A}(m) = \overline{a}(m)\right\} &= (1-p)\overline{a}(m) , \\
\Pr\left\{\overline{A}(m+1) = \overline{a}(m) \,\middle|\, \overline{A}(m) = \overline{a}(m)\right\} &= p\overline{a}(m)+(1-p)(1-\overline{a}(m)) .
\end{aligned}$$

Now we can define a continuous-time Markov chain $\{\overline{A}(t)\}_{t\geq 0}$ on the unit interval $[0,1]$ by a rescaling of the discrete-time Markov chain $\{\overline{A}(m)\}_{m=0}^{\infty}$ and letting the number of sites $n^2 \to \infty$. These two Markov chains are notationally distinguished only by their time indices. The rescaled time t is m in units of n^2, i.e., $m = \lfloor tn^2 \rfloor$ and $m+1 = \lfloor (t+1/n^2)n^2 \rfloor$. Then by taking $\Delta_t = O(1/n^2)$ and letting

$$\Delta_A = \overline{A}(t+\Delta_t) - \overline{a}(t) = \overline{A}(\lfloor (t+\Delta_t)n^2 \rfloor) - \overline{a}(\lfloor tn^2 \rfloor) ,$$

we get

$$\begin{aligned}
&\Pr\left\{\frac{\Delta_A}{\Delta_t} = \frac{\Delta_a}{\Delta_t} \,\middle|\, \overline{A}(t) = \overline{a}(t)\right\} \\
&\quad = \begin{cases} p\,(1-\overline{a}(t)) + O(\Delta_t) & \text{if } \frac{\Delta_a}{\Delta_t} = 1 \\ (1-p)\overline{a}(t) + O(\Delta_t) & \text{if } \frac{\Delta_a}{\Delta_t} = -1 \\ p\overline{a}(t) + (1-p)(1-\overline{a}(t)) + O(\Delta_t) & \text{if } \frac{\Delta_a}{\Delta_t} = 0 \\ O(\Delta_t) & \text{otherwise} \end{cases} .
\end{aligned} \tag{11}$$

Finally by considering the instantaneous rate of change of the expected fraction of sites in phase 1

$$\frac{d}{dt}\overline{\mathbf{a}}(t) := \lim_{\Delta_t\to 0} \mathbf{E}\left(\frac{\overline{A}(t+\Delta_t) - \overline{A}(t)}{\Delta_t} \,\middle|\, \overline{A}(t)\right)$$

we get the limiting differential equation approximation as

$$n^2 \to \infty, \quad \Delta_t \to 0, \quad \Delta_a \to 0 ,$$

such that

$$\Pr\{\, \Delta_a/\Delta_t \in \{0,-1,+1\}\,\} \to 1$$

based on (11) as follows:

$$\dot{\overline{\mathbf{a}}} = \frac{d}{dt}\overline{\mathbf{a}}(t) = p(1-\overline{\mathbf{a}}(t)) - (1-p)\overline{\mathbf{a}}(t) = p - \overline{\mathbf{a}}(t) ,$$

or simply by

$$\dot{\overline{\mathbf{a}}} = p - \overline{\mathbf{a}} = (1+e^{\sigma-\alpha})^{-1} - \overline{\mathbf{a}} . \tag{12}$$

Given the initial condition $\overline{\mathbf{a}}(0) = \overline{\mathbf{a}}_0$, the analytic solution is

$$\overline{\mathbf{a}}(t) = p + (\overline{\mathbf{a}}_0 - p)e^{-t} = (1+e^{\sigma-\alpha})^{-1} + (\overline{\mathbf{a}}_0 - (1+e^{\sigma-\alpha})^{-1})e^{-t}$$

with only one asymptotically stable fixed point

$$\overline{\mathbf{a}}^* = p = (1+e^{\sigma-\alpha})^{-1} . \tag{13}$$

Thus, $\overline{\mathbf{a}}(t)$ in the above differential equation is the expected fraction of sites in phase 1 at time t in the limit of an infinite toroidal square lattice with $|\mathbb{S}_n| = n^2 \to \infty$ and a realization of the continuous time Markov chain $\{\overline{A}(t)\}_{t\geq 0}$ is $\overline{a}(t)$.

Since $\beta = 0$, the probability of a site being in a given phase is independent of the phases of its neighboring sites. Thus, we can obtain $\overline{\mathbf{b}}(t)$, the expected fraction of bonds, by simply multiplying $\overline{\mathbf{a}}(t)$, the probability of finding a randomly chosen site in phase 1, by itself, i.e.,

$$\overline{\mathbf{b}}(t) = \overline{\mathbf{a}}(t)^2 \text{ and } \overline{\mathbf{b}}^* = (\overline{\mathbf{a}}^*)^2 . \tag{14}$$

3.2. Interactive case with $\beta \neq 0$

If $\beta \neq 0$ then the probability of site s being in phase 1 at time $m+1$ depends on the configuration of the neighboring sites of s at time m through $X_{N_s}(m) = \sum_{r \in N_s} X_r(m)$, the number of neighboring sites of s in phase 1 at time m.

$$\begin{aligned}
&\Pr\{X_s(m+1) = x_s(m+1) \,|\, X(m) = x(m)\} \\
&\quad = \Pr\{X_s(m+1) = x_s(m+1) \,\big|\, X_{N_s}(m) = i\} \\
&= \begin{cases} p_i = \left(1 + e^{\sigma - \alpha - i\beta}\right)^{-1} & \text{if } x_s(m+1) = 1 \\ 1 - p_i = 1 - \left(1 + e^{\sigma - \alpha - i\beta}\right)^{-1} & \text{if } x_s(m+1) = 0 \\ 0 & \text{if } x_s(m+1) \notin \{0,1\} \end{cases} .
\end{aligned}$$

Thus the probability that the phase changes from 0 to 1 in one time-step at site s given that $a(m)$ is the total number of sites in phase 1 at time m is

$$\begin{aligned}
&\Pr\{X_s(m+1) = 1, X_s(m) = 0 \,|\, S = s, A(m) = a(m)\} \\
&\quad = \sum_{i=0}^{4} \Pr\{X_s(m+1) = 1, X_{N_s}(m) = i, X_s(m) = 0 \\
&\qquad\qquad\qquad\qquad\qquad\qquad |\, S = s, A(m) = a(m)\} \\
&= \sum_{i=0}^{4} \Pr\{X_s(m+1) = 1 \,\big|\, X_{N_s}(m) = i, \\
&\qquad\qquad \underbrace{X_s(m) = 0, S = s, A(m) = a(m)}_{p_i} \\
&\qquad \times \Pr\{X_{N_s}(m) = i \,\big|\, X_s(m) = 0, S = s, A(m) = a(m)\} \\
&\qquad\quad \times \underbrace{\Pr\{X_s(m) = 0 \,|\, S = s, A(m) = a(m)\}}_{(n^2 - a(m))/n^2 = 1 - \overline{a}(m)}
\end{aligned}$$

Since there are $4!/((4-i)!i!)$ distinct neighborhood configurations with i of the four nearest neighbors of site s in phase 1, we can make the following binomial approximation for $\Pr\{X_{N_s}(m) = i \,\big|\, X_s(m) = 0, S = s, A(m) = a(m)\}$ in the above expression and obtain

$$\begin{aligned}
&\Pr\{X_s(m+1) = 1, X_s(m) = 0 \,|\, S = s, A(m) = a(m)\} \\
&\quad = \sum_{i=0}^{4} p_i (1 - \overline{a}(m)) \\
&\qquad \times \Pr\{X_{N_s}(m) = i \,\big|\, X_s(m) = 0, S = s, A(m) = a(m)\} \\
&\qquad \approx\!\approx \sum_{i=0}^{4} p_i \,(1 - \overline{a}(m)) \binom{4}{i} (\overline{a}(m))^i \,(1 - \overline{a}(m))^{4-i} \quad .
\end{aligned}$$

Therefore, the probability that the total number of sites in phase 1 increases by 1 in one time-step is obtained by adding the probability of a transition from phase 0 to phase 1 over every uniformly chosen site s as follows:

$$\begin{aligned}
&\Pr\{A(m+1) = a(m) + 1 \,|\, A(m) = a(m)\} \\
&= \sum_{s \in \mathbb{S}_n} \Pr\{X_s(m+1) = 1, X_s(m) = 0, S = s \,|\, A(m) = a(m)\} \\
&= \sum_{s \in \mathbb{S}_n} \Pr\{X_s(m+1) = 1, X_s(m) = 0 \,|\, S = s, A(m) = a(m)\} \\
&\qquad\qquad \times \underbrace{\Pr\{S = s \,|\, A(m) = a(m)\}}_{1/n^2} \\
&\approx\!\approx \sum_{s \in \mathbb{S}_n} \left(\sum_{i=0}^{4} p_i \,(1 - \overline{a}(m)) \binom{4}{i} (\overline{a}(m))^i \,(1 - \overline{a}(m))^{4-i} \right) \frac{1}{n^2} \\
&\qquad\qquad = (1 - \overline{a}(m)) \sum_{i=0}^{4} p_i \binom{4}{i} (\overline{a}(m))^i \,(1 - \overline{a}(m))^{4-i} \quad .
\end{aligned}$$

Dividing both sides of the equality that defines the above event by n^2 we get

$$\begin{aligned}
&\Pr\left\{\overline{A}(m+1) = \overline{a}(m) + 1/n^2 \,\big|\, \overline{A}(m) = \overline{a}(m)\right\} \\
&\qquad\qquad \approx\!\approx (1 - \overline{a}(m)) \sum_{i=0}^{4} p_i \binom{4}{i} (\overline{a}(m))^i \,(1 - \overline{a}(m))^{4-i} \quad .
\end{aligned}$$

By an analogous argument we can obtain the probability that $\overline{A}(m+1)$ decreases by $1/n^2$ as

$$\begin{aligned}
&\Pr\left\{\overline{A}(m+1) = \overline{a}(m) - 1/n^2 \,\big|\, \overline{A}(m) = \overline{a}(m)\right\} \\
&\qquad\qquad \approx\!\approx \overline{a}(m) \sum_{i=0}^{4} (1 - p_i) \binom{4}{i} (\overline{a}(m))^i \,(1 - \overline{a}(m))^{4-i} \quad .
\end{aligned}$$

Using the same limiting approximation in the previous Section we can obtain the following differential equation approximation for $\overline{\mathbf{a}} = \overline{\mathbf{a}}(t)$

$$\begin{aligned}
\dot{\overline{\mathbf{a}}} &= \frac{d}{dt}\overline{\mathbf{a}}(t) \\
&= (1 - \overline{\mathbf{a}}) \Big(p_0 (1 - \overline{\mathbf{a}})^4 + p_1 \, 4\overline{\mathbf{a}}(1 - \overline{\mathbf{a}})^3 \\
&\qquad + p_2 \, 6\overline{\mathbf{a}}^2 (1 - \overline{\mathbf{a}})^2 + p_3 \, 4\overline{\mathbf{a}}^3 (1 - \overline{\mathbf{a}}) + p_4 \, \overline{\mathbf{a}}^4 \Big) \\
&\qquad - \overline{\mathbf{a}} \Big((1 - p_0)(1 - \overline{\mathbf{a}})^4 + (1 - p_1) \, 4\overline{\mathbf{a}}(1 - \overline{\mathbf{a}})^3 \\
&\qquad + (1 - p_2) \, 6\overline{\mathbf{a}}^2 (1 - \overline{\mathbf{a}})^2 + (1 - p_3) \, 4\overline{\mathbf{a}}^3 (1 - \overline{\mathbf{a}}) \\
&\qquad + (1 - p_4) \, \overline{\mathbf{a}}^4 \Big) \quad .
\end{aligned}$$

This simplifies after factoring and extracting coefficients of $\overline{\mathbf{a}}$ as follows:

$$\begin{aligned}
\dot{\overline{\mathbf{a}}}(t) &= p_0 - (4\,p_0 - 4\,p_1 + 1)\overline{\mathbf{a}} + 6\,(p_0 - 2\,p_1 + p_2)\overline{\mathbf{a}}^2 \\
&\qquad - 4\,(p_0 - 3\,p_1 + 3\,p_2 - p_3)\overline{\mathbf{a}}^3 \\
&\qquad + (p_0 - 4\,p_1 + 6\,p_2 - 4\,p_3 + p_4)\overline{\mathbf{a}}^4 \quad . \qquad (15)
\end{aligned}$$

We can understand (15) directly as a quartic polynomial in $\overline{\mathbf{a}}$ whose coefficients are given by an alternating binomial series corresponding to the increase and decrease in $\overline{\mathbf{a}}$ based on a combinatorial averaging over the transition diagram of site configurations at the four nearest neighbors of a given site. Next we

characterize the qualitative asymptotic dynamics of the above nonlinear differential equation which reduces to the differential equation (12) if $\beta = 0$ and thereby $p = p_0 = p_1 = p_2 = p_3 = p_4$.

If the externally applied stress σ is beyond α by 2β, i.e.

$$\tilde{\sigma} = \sigma - \alpha = 2\beta \ ,$$

then the probability of being in phase 1 or phase 0 at a site that is surrounded by two neighbors in phase 1 and the other two in phase 0 is equal and exactly half:

$$p_2 = \frac{1}{1 + \exp(\tilde{\sigma} - 2(\tilde{\sigma}/2))} = \frac{1}{2} = 1 - p_2 \ .$$

If we study the system along $\tilde{\sigma} = 2\beta$, the symmetric set of parameters, then

$$p_1 + p_3 = \frac{1}{1 + e^{\tilde{\sigma}/2}} + \frac{1}{1 + e^{-\tilde{\sigma}/2}} = 1 \ ,$$

and also

$$p_0 + p_4 = \frac{1}{1 + e^{\tilde{\sigma}}} + \frac{1}{1 + e^{-\tilde{\sigma}}} = 1 \ .$$

Thus, the coefficient of $\overline{\mathbf{a}}^4$ in (15) vanishes when $\tilde{\sigma} = 2\beta$:

$$p_0 - 4\,p_1 + 6\,p_2 - 4\,p_3 + p_4 = (p_0 + p_4) - 4(p_1 + p_3) + 6p_2 = 0 \ .$$

Therefore, along $\tilde{\sigma} = 2\beta$ our (15) is really just a cubic function of $\overline{\mathbf{a}}$ as opposed to a quartic. The discriminant of this cubic is

$$\Delta_3(\tilde{\sigma},\beta) = 18c_3c_2c_1c_0 - 4c_2^3c_0 + c_2^2c_1^2 - 4c_3c_1^3 - 27c_3^2c_0^2 \ ,$$

where $c_i = c_i(\tilde{\sigma},\beta)$ is the coefficient of $\overline{\mathbf{a}}^i$ in (15), and it takes negative values when $\tilde{\sigma} \in (0, 2.589145)$ (giving one real and two complex conjugate roots), takes positive values when $\tilde{\sigma} < 0$ and $\tilde{\sigma} > 2.589145$ (giving three distinct real roots) and takes 0 when $\tilde{\sigma} \in \{0, 2.589145\}$ (giving three multiple real roots) as shown in Fig. 2.

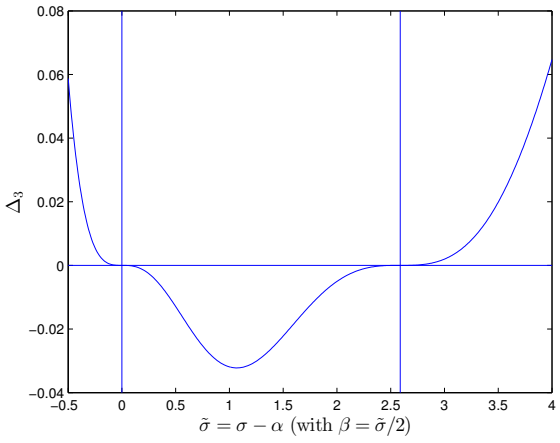

Figure 2: Discriminant Δ_3 of the cubic function of $\overline{\mathbf{a}}$ along $\beta = \tilde{\sigma}/2$ as a function of $\tilde{\sigma} = \sigma - \alpha$.

A sign analysis of the discriminant of the quartic with sixteen terms:

$$\begin{aligned}\Delta_4(\tilde{\sigma},\beta) = {} & 256c_4^3c_0^3 - 192c_4^2c_3c_1c_0^2 - 128c_4^2c_2^2c_0^2 \\ & + 144c_4^2c_2c_1^2c_0 - 27c_4^2c_1^4 + 144c_4c_3^2c_2c_0^2 - 6c_4c_3^2c_1^2c_0 \\ & - 80c_4c_3c_2^2c_1c_0 + 18c_4c_3c_2c_1^3 + 16c_4c_2^4c_0 - 4c_4c_2^3c_1^2 \\ & - 27c_3^4c_0^2 + 18c_3^3c_2c_1c_0 - 4c_3^3c_1^3 - 4c_3^2c_2^3c_0 + c_3^2c_2^2c_1^2\end{aligned}$$

and the three associated polynomials:

$$\begin{aligned} D_4(\tilde{\sigma},\beta) &= 64c_4^3c_0 - 16c_4^2c_2^2 + 16c_4c_3^2c_2 \\ &\quad -16c_4^2c_3c_1 - 3c_3^4 \\ \Delta_0(\tilde{\sigma},\beta) &= 256c_2^2 - 3c_3c_1 + 12c_4c_0 \\ P_4(\tilde{\sigma},\beta) &= 8c_4c_2 - 3c_3^2 \ , \end{aligned}$$

shows that the four real distinct roots occur inside the shaded region of the parameter space in the left panel of Fig. 3 where $\Delta_4 > 0$, $P_4 < 0$ and $D_4 < 0$.

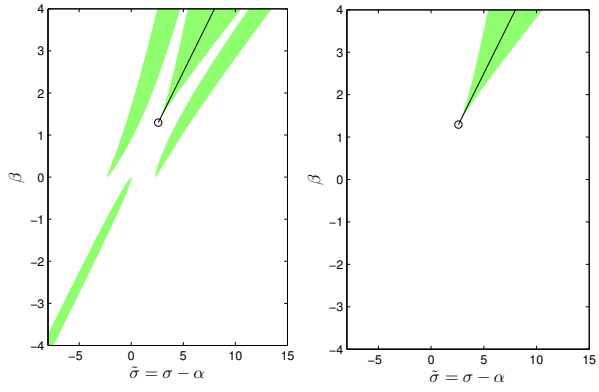

Figure 3: Four real roots of the quartic occur in the shaded region over $\tilde{\sigma} = \sigma - \alpha$ and $\beta = \tilde{\sigma}$ is shown in the left panel. The black line is $\beta = \tilde{\sigma}/2$ started at $(2.589145, 2.589145/2)$. The parameter space with only three distinct real roots in $[0, 1]$ is shown in the right panel.

The entire shaded region in the right panel of Fig. 3, containing the black line started at $(2.589145, 2.589145/2)$ with multiple real root, has three distinct real roots inside $[0, 1]$ while the other three shaded regions in the left panel of Fig. 3 only contain one of the four distinct real roots in $[0, 1]$. Analysis of the derivative at the roots corresponding to each $(\tilde{\sigma},\beta)$ in the shaded region on the right panel of Fig. 3 shows that only one of the three distinct real roots is an unstable fixed point while the other two roots are stable fixed points of the ODE in (15). This naturally corresponds to a family of pitch-fork bifurcations and the associated hysteresis depending on where the system is initialized from. The unshaded region in the left panel of Fig. 3 corresponds to the parameter space where the quartic discriminant Δ_4 is negative and thus implying the existence of two real roots (with one of them in $[0, 1]$) and two complex conjugate roots. The real roots and their derivatives over each $(\tilde{\sigma},\beta)$ in a grid of parameter values from $[-8, 12] \times [-4, 4]$ were obtained through interval analytic methods using [33].

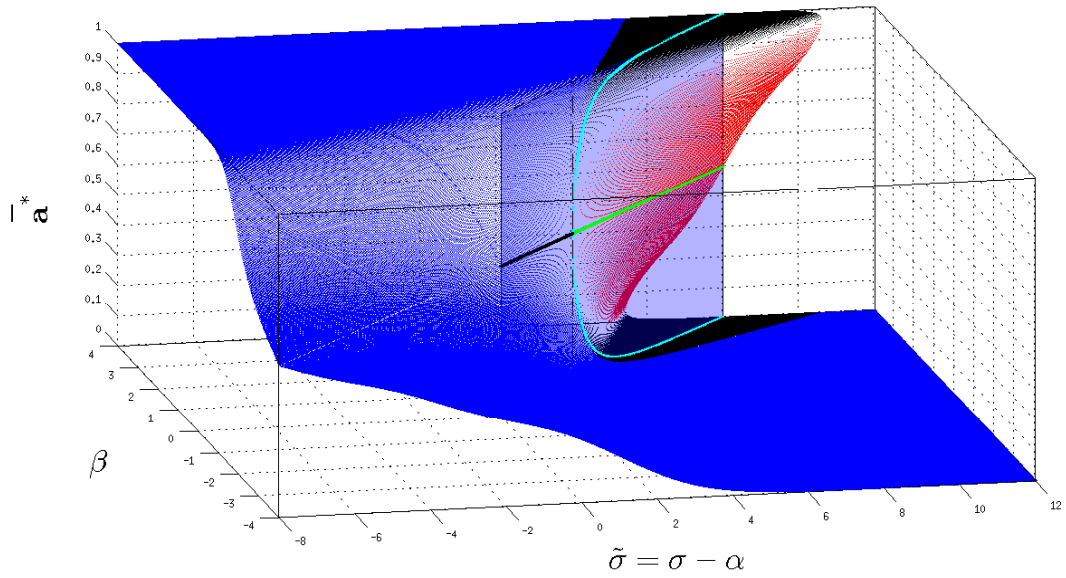

Figure 4: The fixed points $\bar{\mathbf{a}}^*$ as a set-valued function of the parameters $\tilde{\sigma} = \sigma - \alpha$ and β. The blue, black and azure points are the stable fixed points while the red and green points are the unstable fixed points of the system. There is a pitch-fork bifurcation along $\tilde{\sigma} = 2\beta$ that starts at $(2.589145, 1.2945725)$ where the fixed point at 0.5 becomes unstable with two stable fixed points on either side.

Figure 4 shows the set of fixed points $\bar{\mathbf{a}}^*$ of the system as a function of $(\tilde{\sigma}, \beta)$. The parameter space corresponding to the central shaded region of Fig. 3 containing the line $\beta = \tilde{\sigma}/2$ is evident in Fig. 4 with three fixed points in $[0, 1]$. The pitch-fork bifurcations along the plane $\tilde{\sigma} = 2\beta$ or $\beta = \tilde{\sigma}/2$ determined by the non-negative sign of the cubic discriminant of Fig. 2 along the black line in Fig. 3 is displayed to highlight the dynamics with one unstable fixed point at $1/2$ and two other stable fixed points that are equi-distant on either side of $1/2$.

We are interested in varying the externally applied stress σ for a given material characterized by fixed rheological parameters α and β. This amounts to varying $\tilde{\sigma}$ for a fixed β since the fixed α is absorbed into $\tilde{\sigma} = \sigma - \alpha$. The asymptotic dynamics when we apply a constant external stress for a long period of time are given by the fixed points $\bar{\mathbf{a}}^*$ in Fig. 4. We study such stress-dependent behavior from the Gibbs sampler and compare it with ODE approximation in the next Section. Note that the ODE model for $\beta \neq 0$ is only in qualitative agreement with $\bar{\mathbf{a}}(t)$, the expected volume fraction of the unyielded material at time t. This is because we are ignoring the dependent statistic $\bar{\mathbf{b}}(t)$, the expected fraction of bonds or pairs of neighboring unyielded material at time t. Despite this simplification, as we will see in Sec. 4, there is qualitative agreement between the ODE and the Gibbs simulations. Furthermore, an admittedly *ad hoc* correction of the ODE through a translation of the vector field by (α_0, β_0) even improves the quantitative approximation. We postpone a formal quantitative approximation of the ODE using perturbation theoretic methods to the future and focus here on obtaining insights from the Gibbs sampler that is in qualitative agreement with the ODE approximation.

4. Results

In this Section we mainly obtain various insights about the macroscopic behavior of our model based on Monte Carlo simulations from Algorithms 1 and 2 and make some comparisons with the approximating nonlinear ODE model of Sec. 3.

4.1. Behavior under zero stress

In the absence of any external stress, we are interested in the macroscopic behavior of phase transition from an initial fluid configuration, typically with $x(0) = \mathbf{0}$, to the configuration of a physical gel with a percolation cluster. Recall from Sections 2.5 and 2.6.1 that a percolation cluster appears when the largest connected component of the configuration x given by $C_x^{(*)}$ spans the entire lattice as indicated by $F_x^{(*)} = 1$. This process is known as *aging* and can be thought of as the process of letting the material rest after having agitated it to a fully fluid state.

Let the initial site configuration be all fluid with $x(0) = \mathbf{0}$ and $(\bar{a}(x(0)), \bar{b}(x(0))) = (0, 0)$. We model aging by the time evolution of the site configuration, i.e. by $x(m)$ as $m \to \infty$, or equivalently in rescaled time by $x(t)$ as $t \to \infty$, where $m = \lfloor tn^2 \rfloor$. The material as it ages may or may not form a gel depending on the parameters α and β. For various values of α and β we will first obtain insights from Monte Carlo simulations of stress-free gelation, i.e., for the fluid-solid (F-S) phase transition to occur in the absence of external stress, and then compare them with the ODE approximation.

Site percolation model of Sec. 2.6.1 with *site-filling probability* p, which gives the probability of a site being in phase 1, has been used (see [28, 34] and references therein) to model gelation over time. In these studies percolation transition as p

varies is used to model gel transition. In our approach we treat α, the site-specific threshold, and β, the interaction constant, as fixed rheological parameters that characterize the nature of the given yield stress material. Recall that α and β specify the Gibbs potential over the two types of cliques in order to give the energy of a site configuration under a given external stress σ (as derived in Sec. 2). When we study the possible gelation of a material with a given α and β we do not think of varying the site-filling probability directly, as in [34], but rather let it be defined by α and β in a possibly configuration-dependent manner. Thus, if we find that gelation occurs for a specific value of (α,β), say $(8,1)$, then we interpret this as the gelation of the material with $(\alpha,\beta) = (8,1)$ in the absence of external stress, i.e. the material evolves probabilistically on the configuration space from the completely fluid configuration of $\mathbf{0}$ to one with a percolation cluster. Thus our approach to modeling gelation is not only microscopic but also mechanistic, in terms of allowing the nature of stochastic evolution in the configuration space to depend on the fixed rheological parameters α and β.

Recall that our non-interactive model with $\beta = 0$, in the absence of any external stress ($\sigma = 0$), is the site percolation model with site-filling probability $p = (1+e^{-\alpha})^{-1}$. When $\beta = 0$ and $p = (1+e^{-\alpha})^{-1} \geq p_c \approxeq 0.5927$, the critical site percolation probability, we have a large *percolation cluster* of gelled sites that permeates through out the material and turns the material into a gel. If $(1+e^{-\alpha})^{-1} < p_c$ then the material, as it ages, will not form a percolation cluster and therefore remain as a fluid. The critical value p_c of the site-filling probability p can be transformed into a critical value α_c of the rheological parameter α, in the absence of interaction ($\beta = 0$) and external stress ($\sigma = 0$) as follows:

$$\alpha \geq \alpha_c = -\ln(p_c^{-1}-1) = -\ln(0.5927^{-1}-1) \approxeq 0.37513 \ . \quad (16)$$

Thus, if $\beta = 0$, $\sigma = 0$ and the rheological parameter $\alpha \geq \alpha_c$ then the material will cross the *bulk gel point* and turn into a solid on the basis of the classical site percolation model. On the other hand, if $\beta = 0$, $\sigma = 0$ and $\alpha < \alpha_c$ then it will remain as a fluid.

Figure 5 compares five realizations of $\overline{A}(t)$ and $\overline{B}(t)$ from the Gibbs Sampler with their respective expectations $\overline{\mathbf{a}}(t)$ and $\overline{\mathbf{b}}(t)$, when $\beta = 0$, as derived in (12), (13) and (14), for the initial condition $\overline{\mathbf{a}}(0) = \overline{\mathbf{a}}_0 = 0$ based on the site configuration being initialized at the all-zero state $x(0) = \mathbf{0}$ in the absence of any external stress. Figure 5 shows the approximating ODE solutions for the expectation as black lines (plain for $\overline{\mathbf{a}}(t)$ and dashed for $\overline{\mathbf{b}}(t)$ with thin lines for $\alpha = 0.2$ and thick lines for $\alpha = 2.0$) and five of the corresponding realizations of $\overline{A}(t)$ and $\overline{B}(t)$ as oscillating gray trajectories that are concentrated about them. The trajectory of $\overline{\mathbf{a}}(t)$ (the thin black line of Fig. 5) when $\alpha = 0.2 < \alpha_c$ and $\beta = 0$ does not form a gel, i.e. $\Pr\{F_X^{(*)} = 1\} = 0$, because the site-filling probability $p = 1 + e^{-0.2} = 0.549834$ (which is also the fixed point, i.e., $\overline{\mathbf{a}}^* = p$) is below the critical site percolation probability $p_c \approxeq 0.5927$. On the other hand, the trajectory of $\overline{\mathbf{a}}(t)$ (the thick black line of Fig. 5) when $\alpha = 2 \geq \alpha_c$ forms a gel, i.e. $\Pr\{F_X^{(*)} = 1\} > 0$, since the site-filling probability $p = \overline{\mathbf{a}}^* = 1 + e^{-2} \approxeq 0.8808$ is greater than p_c. Figure 5 shows

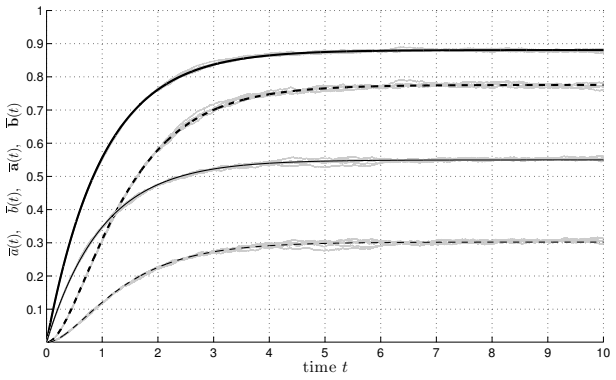

Figure 5: Plots of five simulated realizations $\overline{a}(t)$ and $\overline{b}(t)$ of the configuration statistics $\overline{A}(t)$ and $\overline{B}(t)$ as a function (gray line) of rescaled simulation time t (in units of $n^2 = 10^4$) when external stress $\sigma = 0$, initial condition $\mathbf{0}$, $\beta = 0$ and two values for $\alpha \in \{0.2, 2.0\}$. The approximating solutions for the expectation are shown as black lines (plain for $\overline{\mathbf{a}}(t)$ and dashed for $\overline{\mathbf{b}}(t)$ with thin lines for $\alpha = 0.2$ and thick lines for $\alpha = 2.0$).

agreement between $\overline{\mathbf{a}}(t)$, the ODE-based approximation of the expected fraction of sites in phase 1, and the sample mean of five independent realizations of $\overline{A}(t)$ using Algorithm 1 even when $n^2 = 10^4$ and improves further when we double n with $n^2 = 4 \times 10^4$ (results not shown here). Figure 5 also shows a similar agreement between $\overline{\mathbf{b}}(t)$ and five independent realizations of $\overline{B}(t)$. Thus, if $\beta = 0$ then the ODE model given by (12), (13) and (14) captures the expectation of $\overline{A}(t)$ and $\overline{B}(t)$ given by the rescaled Markov chain $\{X(t)\}_{t\geq 0}$.

If $\beta > 0$ then our model, being a particular parametric family of correlated site percolation, allows for the site-filling probability p_i at site s to be site-specific by making it depend on $i = x_{N_s}$, the number of neighboring sites of s that are in phase 1. Thus, the site-filling probability changes site-specifically with the configuration $x(m)$ at time m. If $\beta \geq 0$ and $\alpha > \alpha_c$ then p_i, the site-filling probability at every site s, in the absence of any external stress ($\sigma = 0$), is at least as high as the critical percolation probability p_c. This is sufficient for the formation of the percolation cluster and attain stress-free gelation. Recall that p_c for site percolation is not known analytically but estimated consistently from Monte Carlo simulations even when $\beta = 0$. We can similarly obtain Monte Carlo estimates of a bi-partition of a large subset of the parameter space, say $\{(\alpha,\beta) : \alpha \in [10^{-4}, 10] \times [10^{-4}, 10]\}$, into a *gellable* subset of parameters that lead to the formation of a gel and another *ungellable* subset of parameters that do not, using Algorithm 1.

For a given parameter value (α,β) in a set made from the union of logarithmically, linearly and quasi-randomly spaced points in $[10^{-4}, 10]^2$ we can simulate site configurations $x(m)$ according to Algorithm 1 with $\sigma = 0$ and initial fluid configuration $x(0) = \mathbf{0}$ as m approaches a large number, say 10^6. Figure 6 shows, over a grid of parameters in $[10^{-4}, 10]^2$, the nearly asymptotic value of $F_{x(100)}^{(*)}$, the proportion of the lattice with $n^2 = 10^4$ sites that is occupied by the largest cluster (connected component) of gelled sites at a large discrete time $m = 10^6$ or rescaled time $t = 100$ after each site has undergone $h = 100$

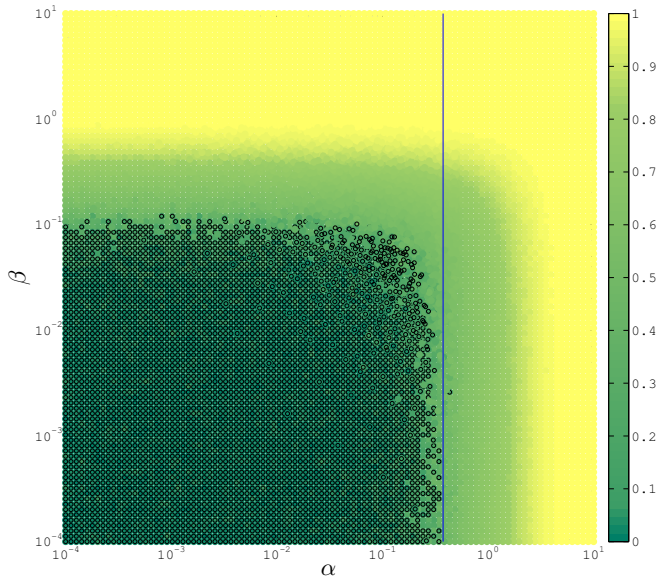

Figure 6: The shading of the circle at each (α,β) indicates $F^{(*)}_{x(100)}$, the proportion of the lattice occupied by the largest cluster of gelled sites at rescaled time $t = 100$ after having initialized from the all fluid configuration $\mathbf{0}$ in the absence of external stress. Parameter values that do not lead to a percolation cluster after each one of the $n^2 = 10^4$ sites has undergone 100 transitions (on average), i.e. with $F^{(*)}_{x(100)} < 1$, are highlighted by circles with black boundary.

transitions on average. The set of *ungellable* parameters are estimated to be those whose $F^{(*)}_{x(100)} < 1$ and are highlighted by circles with black boundaries in the lower left corner of Fig. 6. The set of parameters with $F^{(*)}_{x(100)} = 1$ are estimated to be *gellable* and depicted in Fig. 6 by shaded circles without a black boundary. These estimates are only based on one simulation per (α,β) and just meant to give a rough idea of gel formation. However, the characteristics of the bi-partition of the parameter space into gellable and ungellable regions are similar to Figure 6 when we increased the lattice size n from 100^2 to 200^2 and the duration t from 100 to 200 (results not shown). By doing multiple independent simulations per parameter value over a larger lattice ($n > 10^4$) and longer time ($t > 100$) one can easily obtain asymptotically consistent estimates (with standard errors) for the (α,β)-specific probability that $F^{(*)}_{x(t)} = 1$ as $t \to \infty$ and $n \to \infty$ using Algorithm 1.

From Figure 6 it is clear that the material gets gelled in the absence of external stress not only when $\alpha > \alpha_c \approxeq 0.37513$ (the vertical line in Fig. 6 goes through α_c) but also for smaller values of α, provided β is large enough to compensate and increase the site-filling probability. In the sequel, we are mainly interested in values of α much larger than α_c, say $\alpha = 8$ without loss of generality, in order to focus on yield stress materials that can form a gel with a high probability under zero stress. This concludes our study of *stress-free gelation*, i.e. the possibility of a fluid to solid phase transition under zero external stress.

4.2. Behavior under constant stress

We are interested in the effect of applying constant external stress σ for a long period of time to an yield stress material with rheological properties specified by parameters α and β. The value of $\overline{\mathbf{a}}(t)$, the expected fraction of gelled material at time t, as t approaches infinity under a constant external stress σ for a fixed value of α and β, i.e., for a fixed value of $(\tilde{\sigma},\beta)$ since $\tilde{\sigma} = \sigma - \alpha$, is given by the fixed point(s) of the multi-valued map $\overline{\mathbf{a}}^*(\tilde{\sigma},\beta)$ depicted in Fig. 4 on the basis of the approximating ODE for $\overline{\mathbf{a}}(t)$ in (15).

The left (and middle) sub-plot of Fig. 7 approximates the time asymptotic behavior of $\overline{a}$ when the Monte Carlo simulation of Gibbs field was initialized from $\mathbf{1}$ (and from $\mathbf{0}$) using Algorithm 1 with $h = 100$, $n = 100$ and $(\tilde{\sigma},\beta)$ taken from a grid of linearly spaced points in $[-10, 15] \times [0, 4]$. The difference in $\overline{a}$ between the left and middle sub-plots of Fig. 7 is shown as the triangular region of hysteresis with value 1 in the right sub-plot where $\overline{a}$ initialized from $\mathbf{1}$ is 1 more than $\overline{a}$ initialized from $\mathbf{0}$ after a large amount of rescaled time ($t = 100$) has elapsed and the system is in its steady state. The ODE model is in qualitative agreement with these Monte Carlo simulations from the Gibbs field model due to the presence of a similar triangular region of hysteresis in the right panel of Fig. 3 that contains three real roots in $[0, 1]$ or from the folded region with three fixed points in the multi-valued map of Fig. 4. For example from this ODE approximation we know that hysteresis can only occur if the agglomerative interaction parameter $\beta > \beta_h \approxeq 1.2945725$. The value of β_h based on the Monte Carlo simulations of the Gibbs field is not much larger than 1.2945725 (for $n = 100$ and $t = 100$ we notice the presence of a strong hysteretic effect for values of $\beta > 1.5$).

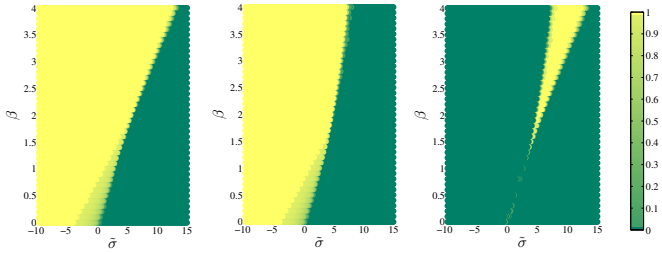

Figure 7: The value of $\overline{a}$ at rescaled time $t = 100$ from Monte Carlo simulations of the Gibbs field using Algorithm 1 for fixed parameters $(\tilde{\sigma},\beta)$ when initialized from $\mathbf{1}$ (left subplot) and from $\mathbf{0}$ (middle sub-plot). The difference in $\overline{a}$ between left and middle sub-plots is shown in the right sub-plot.

4.3. Configurations at the Solid-Fluid Interface

From the ODE model (Fig. 4) as well as the Gibbs sampler (Fig. 7) it is clear that for smaller values of β, say $\beta < 1.5$, as the stress σ applied upon the material, that is initialized from $\overline{a} = 1$ (or from $\overline{a} = 0$), increases (or decreases) for a fixed α, i.e. as $\tilde{\sigma}$ increases (or decreases), the transition in the steady state value of $\overline{a}$ from 1 to 0 (or from 0 to 1) is less abrupt when compared to the transition for larger values of β. This is due to the effect of the unstable fixed point in the interior of $[0, 1]$ and the two

stable fixed points close to the boundaries of $[0, 1]$. We are interested in the nature of the configuration x for a given β at the solid-fluid interface, i.e. when $\overline{a} = 1/2$, as $\tilde{\sigma}$ reaches a specific value. Site configurations at the solid-fluid interface provide the random environment for restricted diffusion of small tracer particles near gel transition. This phenomenon is of experimental and theoretical interest [22, 23, 10] and has been recently studied for the case of $\beta = 0$ [34]. We are interested here in gaining insights on the nature of the site configurations at the solid-fluid interface for values of β below, above and equal to zero.

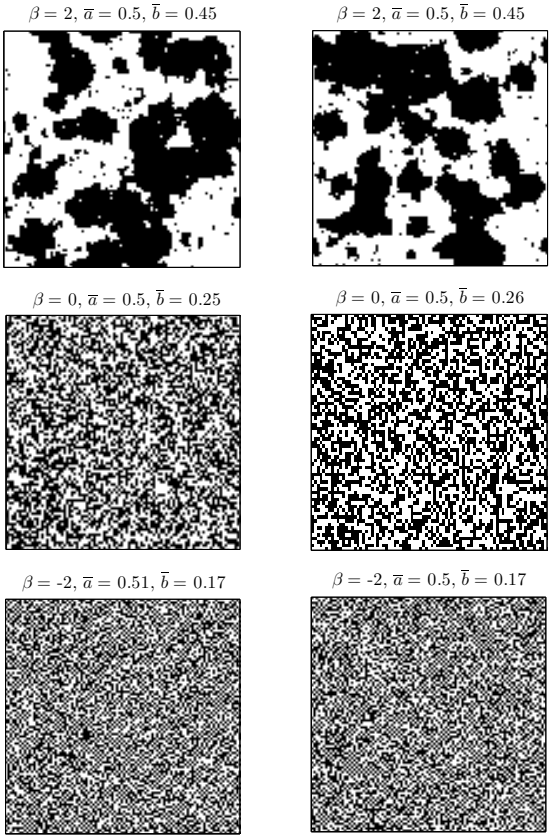

Figure 8: Effect of β on preferred energy minimizing configurations. Two sample configurations are shown for each $\beta \in \{-2, 0, +2\}$ over a toroidal square lattice of 100×100 sites. Sites in phase 0 and 1 are shown in black and white, respectively, at the solid-fluid interface when $\overline{a} \approxeq 1/2$.

Figure 8 shows two random site configurations at the solid-fluid interface when $\overline{a} \approxeq 1/2$ for three different values of β. Without loss of generality, we fixed $\alpha = 8$, and focus on the properties of the material that is capable of forming a gel in the absence of external stress. Clearly, the site configurations are dependent on the magnitude and sign of the interaction parameter β. Recall that $\overline{a}$, the fraction of gelled sites, and $\overline{b}$, the fraction of pairs of neighboring gelled sites, are the sufficient statistic of the configuration, i.e. the energy of the configuration only depends on its $(\overline{a}, \overline{b})$.

4.3.1. Configurations when $\overline{a} \approxeq 1/2$ and $\beta = 0$

If $\beta = 0$, the non-interactive case of the classical site percolation model studied in [34], and $\tilde{\sigma}$ is chosen so that $\overline{a} = 1/2$ then due to the site-filling probability being independently and identically distributed across all n^2 sites $\overline{b} = \overline{a}^2 = 1/4$. Two typical configurations when $\beta = 0$, $n = 100$ and $t = 100$ at the solid-fluid interface are shown by the sub-plots in the second row of Fig. 8. More configurations were visually explored and their distinguishing site configuration feature is characterized by the independence of the site-filling probability over sites and is apparent by the concentration of their sufficient statistics $(\overline{a}, \overline{b})$ about $(\overline{a}, \overline{a}^2) = (1/2, 1/4)$ at the solid-fluid interface. This is the only case considered by [34] when obtaining the random environment for restricted diffusion of small tracer particles near gel transition.

4.3.2. Configurations when $\overline{a} \approxeq 1/2$ and $\beta = 2$

When we increase β from 0 to 2 we have a very different distribution over site configurations at the solid-fluid interface as shown by two samples in the first (top) row of Fig. 8. It is easy to understand this "patchy" pattern in site configurations with large positive β by realizing that new gelled sites can occur with a higher probability at sites neighboring existing gelled sites that have a larger $i = x_{N_s}$, number of neighbors in phase 1, than at sites surrounded by ungelled sites with a smaller $i = x_{N_s}$ (see bottom two rows of Fig. 1). As β gets larger, the probability of forming gelled sites around existing gelled sites is much larger than that of forming gelled sites around ungelled sites, and this concentrates $(\overline{a}, \overline{b})$ about $(\overline{a}, \overline{a}) = (1/2, 1/2)$ at the solid-fluid interface.

4.3.3. Configurations when $\overline{a} \approxeq 1/2$ and $\beta = -2$

Finally, when we decrease β from 0 to -2 we have a "checkered" pattern of site configurations at the solid-fluid interface as shown by two samples in the third (bottom) row of Fig. 8. As β gets negative, the probability of forming gelled sites around existing gelled sites gets much smaller (see top row of Fig. 1). In the extreme asymptotic case, as $\beta \to -\infty$, we obtain configurations with increasingly checkered patters with $(\overline{a}, \overline{b}) \to (1/2, 0)$, the sufficient statistics of the extreme "chess board" configuration (such patterns occur already for $\beta = -8$ with $n = 100$ but are not shown here).

Thus, from the β-dependent site configurations at the solid-fluid interface depicted in Fig. 8, it is clear that the trajectories of tracer particles (see Fig. 1 of [10] from [22]) that can only diffuse through the ungelled (black) contiguous regions are heavily dependent on whether there is interaction between adjacent gelled sites. This interaction is captured in our correlated site percolation model by the interaction parameter β.

4.4. Behavior under varying stress

The energy of $X(t)$, the random site configuration at time t, depends on two of its highly correlated statistics: $\overline{A}(t)$, the random fraction of gelled sites at time t, and $\overline{B}(t)$, the random fraction of connected sites at time t. One of our primary interests is to study $\overline{A}(t)$ and $\overline{B}(t)$ as $X(t)$ is under the influence of time-varying externally applied stress $\sigma(t)$.

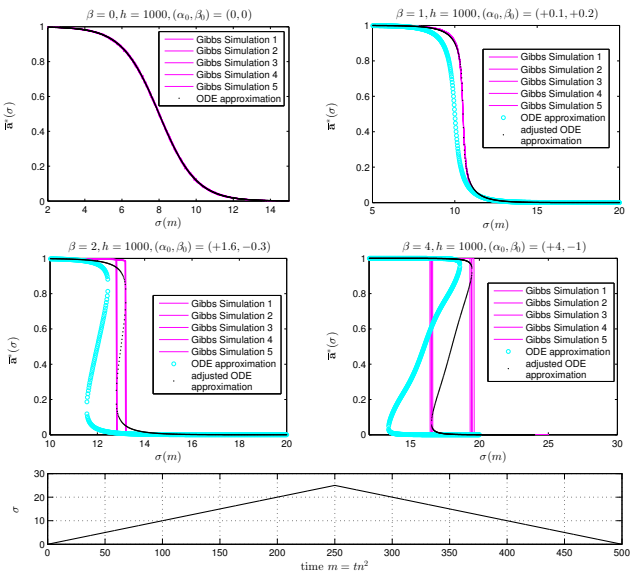

Figure 9: Gibbs field, fixed points of ODE with and without (α_0, β_0)-translation (for progressively higher and lower stresses with $\alpha = 8$ and $\beta \in \{0, 1, 2, 4\}$). The stress was increased from 0 to 25 in units of 0.01 and decreased back to 0 with a holding time of $h = 1000$ (nearly asymptotic state for each distinct stress) as the site configuration varied from **1** to **0** and then back to **1**.

Using Monte Carlo simulations from Algorithm 2 of the time-inhomogeneous Markov chain $\{X(m)\}_{m=0}^{Mh}$ given by (7) and (8), under an initially increasing and subsequently decreasing time-dependent stress $\sigma(m)$ given in the bottom panel of Figure 9, we obtained multiple independent trajectories of $\overline{A}(\sigma)$, the fraction of gelled sites as a function of the external stress σ. Five such simulated trajectories are shown as (pink) thin lines in the first four panels of Figure 9. Note that when $\beta \in \{0, 1\}$ (top row of Figure 9), the value of $\overline{a}(\sigma)$ is only dependent on σ and not on whether the material experienced this value of σ, for a holding time of $h = 1000$ hits per site on average, in the *up-ramp* as we increase $\sigma(m)$ or in the *down-ramp* as we decrease $\sigma(m)$. On the other hand, for values of $\beta \in \{2, 4\}$ (middle row of Figure 9), we notice $\overline{a}(\sigma)$ taking two distinct values over a range of σ values depending on whether σ was experienced in the up-ramp or the down-ramp. In the middle row of Figure 9, $\overline{a}(\sigma)$ reaches the value of $1/2$ under a higher value of σ in the up-ramp as opposed to the down-ramp. This is a clear sign of hysteresis shown by the realizations of the time-inhomogeneous Markov chain under time-dependent stress $\sigma(m)$.

Due the near asymptotic exposure of the material at each stress value for an average of $h = 1000$ hits per site, we can directly compare these stochastic trajectories of $\overline{a}(\sigma)$ (pink thin lines in Figure 9) with that obtained from the fixed point map of $\overline{\mathbf{a}}^*(\sigma - \alpha, \beta)$ in Figure 4 for the approximating ODE model for $\overline{\mathbf{a}}(t)$, the expected fraction of gelled sites, in an (α, β)-specific manner. These ODE-based approximations are given by cyan circles in the first four panels of Figure 9 and are seen to be only in qualitative agreement with the trajectories of $\overline{a}(\sigma)$ since our ODE approximation only models $\overline{\mathbf{a}}$, instead of modelling the dependent pair $(\overline{\mathbf{a}}, \overline{\mathbf{b}})$ that is sufficient for the energy. We do an *ad-hoc* improvement in the ODE-based approximations by a translation of the fixed points map by (α_0, β_0) as shown by black dots in the first four panels of Figure 9. This ad-hoc adjustment is not a substitute for a principled approach based on perturbation theoretic methods that could be pursued in the future.

4.4.1. *Regression of $\overline{B}$ from $\overline{A}$*

The time evolution of the energy-determining statistics $(\overline{A}(t), \overline{B}(t))$ of $X(t)$ can be obtained as $X(t)$ evolves initially from the fully solid phase with $(\overline{A}(0), \overline{B}(0)) = (1, 1)$ towards the fully fluid phase with $(\overline{A}(t), \overline{B}(t)) = (1, 1)$ and back to the fully solid phase under a linearly increasing and subsequently decreasing stress ramp specified by $\sigma(t)$ (as shown at the bottom panel of Fig. 9) according to Algorithm 2. Using multiple independent realizations of such $(\overline{A}(t), \overline{B}(t))$ trajectories (which can be plotted on their phase space $[0, 1] \times [0, 1]$) we can obtain insights into the (α, β)-specific distribution using least-squares regression. For each β we have fitted five simulated trajectories of $\overline{B}$ as a function of $\overline{A}$ when the configuration evolves according to Algorithm 2 under the influence of the stress ramp shown at the bottom panel of Fig. 9.

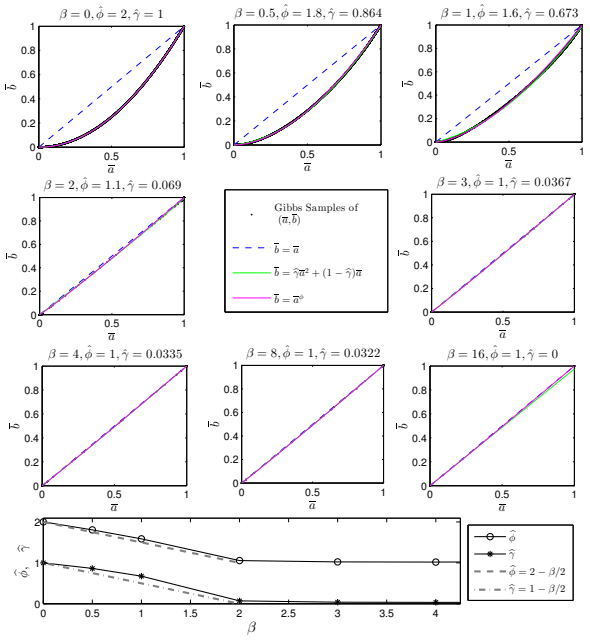

Figure 10: Effect of increasing β on preferred site configurations up to their $(\overline{a}, \overline{b})$ statistics. The stress was increased in units of 0.01 with $h = 1000$ (nearly asymptotic state for each stress) as x varied from **1** to **0** and then back to **1** as stress decreased (with $\alpha = 8$).

Since our ODE approximation only models $\overline{\mathbf{a}}$, instead of modelling the dependent pair $(\overline{\mathbf{a}}, \overline{\mathbf{b}})$ that is sufficient for the energy, we parametrically capture the β-specific relation of $\overline{b}$ to $\overline{a}$ through ordinary least-squares regression. Two functional forms were used to interpolate from $\overline{a}^2$ to $\overline{a}^1$ as β increased from 0 to 16: (i) a polynomial mixture parametrized by $\gamma \in [0, 1]$

$$\overline{b} = \gamma \overline{a}^2 + (1 - \gamma)\overline{a}$$

and (ii) a power law parametrized by $\phi \in [1, 2]$

$$\overline{b} = \overline{a}^{\phi}$$

The least squares estimate of the parameters for each β are $\widehat{\gamma}$ and $\widehat{\phi}$, respectively. The fits are displayed in Fig. 10 and the fitted values as a function of β are displayed in bottom panel. It is clear from the regressions that as β increases from 0, the expectation of $(\overline{A}, \overline{B})$ approaches the identity function $\overline{B} = \overline{A}$ quite quickly. Even for values of $\beta = 2$, we already have realizations with $\overline{b} \approxeq \overline{a}$, under the stress regime shown at the bottom panel of Fig. 9. This is clearly due to the higher probability of forming gelled sites next to sites that are already gelled.

4.4.2. Effect of Holding time on Hysteresis

We next investigate the relationship between the area of the hysteresis given by the trajectory of $\overline{a}$ and the holding time h in an increasing and decreasing stress regime as in the bottom panel of Fig. 9. This is motivated by the finding of a power law relationship between the area of hysteresis and the holding time [10, Figure 11]. In particular we are interested in finding the range of values of β such that the decay in the area of hysteresis for $\overline{a}$, as a function of the holding time t_0 per stress value, is proportional to t_0^1 (as shown in [10, Figure 11]). Here t_0 is determined by h, the average number of hits per site.

Note that although the area of the hysteresis decreases with increased time spent on each stress value (larger h) as evident in Fig. 11, the phase transition under agglomerative interaction with $\beta > 0$ remains abrupt when compared to the more gradual transition for the non-interactive model with $\beta = 0$. This abruptness of the phase transition for positive β is due to the $(\overline{a}(t), \overline{b}(t))$ trajectories of the energy minimizing configuration $x(t)$ getting closer to the $\overline{b} = \overline{a}$ line as β gets large. Moreover, our model allows for a genuine hysteresis in the sense that for values of β larger than about 1.5 the area of the hysteresis will be strictly greater than zero even with infinite holding time at each stress level.

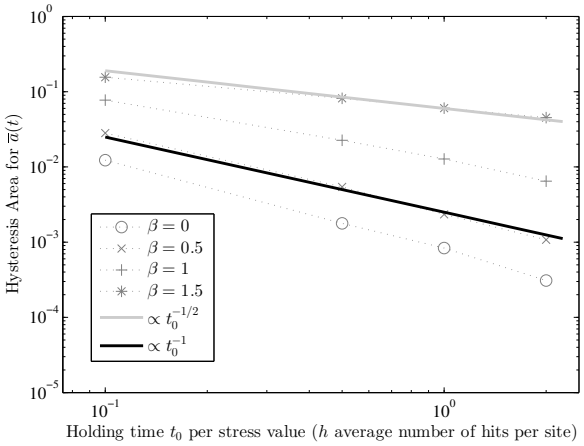

Figure 11: Effect of increasing β on the relative hysteresis area for $\overline{a}$ for different holding times t_0 per stress level in a stress ramp from 0 to 25 in increments of 0.01 (with $\alpha = 8$).

5. Discussion

In summary, using α, a site-specific threshold, β, an interaction constant and σ, an external stress, we derive a thermodynamically consistent correlated site percolation model over a toroidal square lattice. This Markov chain over the space of site configurations can be simulated using Gibbs sampling schemes given by Algorithms 1 and 2. We also derived an approximating nonlinear ODE for the fraction of gelled sites and found the hysteresis present in the ODE in qualitative agreement with the simulations from the Gibbs sampling schemes of the correlated site percolation model.

The simulations from Algorithms 1 and 2 were used to gain several macroscopic insights about yield stress fluids and were found to be in qualitative and quantitative agreement with known empirical results. For example, our model accounts for the effect of non-zero β on preferred site configurations at the solid-fluid interface when $\overline{a} = 1/2$ as shown in Fig. 8. The β-dependent micro-structure of the interface at this bulk gel point clearly influences the motion of the micro-sized tracer particles as studied by [34] (but only for the non-interactive case with $\beta = 0$). For example it is clear from the configurations close to the gel point that a large negative β creates a chess-board pattern of gelled and ungelled sites that would prohibit the motion of tracers from their most recent positions while a large positive β with agglomerative clumping of gelled sites allows more navigable room for the tracers. de Bruyn [34] concludes that their simulations (with $\beta = 0$) do not reproduce the scaling behavior displayed by the microrheological moduli in experiments on materials near their gel point. Although we do not pursue the properties of tracer particle motion at the gel point in this work we expect it to be an interesting future pursuit using non-zero values of β.

We remark that the Gibbs Simulations as well as the approximating ODE are in qualitative agreement with the simple phenomenological macroscopic model for the structural hysteresis proposed in [10, Eqn. (2)]. A more quantitative comparison between these models aimed at highlighting their differences may be useful.

Ideally, perturbation theoretic methods should be used to improve the quantitative agreement between the nonlinear ODE model and the stochastic trajectories as opposed to the ad-hoc translations of the vector field done in this study. A more detailed model that simultaneously represents the fraction of gelled sites and the fraction of bonds in one dependent system would provide a better quantitative and qualitative approximation of the correlated site percolation model.

Another interesting extension of our model could involve allowing for solvent effects through a model akin to *correlated site-bond percolation* of [28, Sec. D.II., p.136] but with our focus on external stress as opposed to temperature. In such a model we have an additional parameter that allows for a site to be occupied by a monomer with probability ϕ and by the solvent with probability $1 - \phi$.

Acknowledgements

This collaborative work commenced during TB's visit to University of Canterbury (UC) in 2012 with partial support from a research grant to MM-G from UC's College of Engineering and by the project ThIM to TB from the National French Research Agency (ANR). RS and MM-G visited Nantes in 2013 with partial support from the project ThIM, the Laboratoire de Thermocinétique (LTN UMR 6607) and research travel grants from UC's College of Engineering. RS thanks Anusha Raazesh for diagrams of neighborhood configurations that led to the binomial approximation in Section 3.2 and Brendan Creutz for discussions on parametrized discriminants of cubic and quartic polynomials.

Appendix A. Algorithms

Here we present the two main algorithms for Gibbs sampling. Algorithm 1 produces a sample path in the space of site configurations under a homogeneous Markov chain with a given initial condition $x(0)$ and rheological parameters α and β, external constant stress σ and holding time h. Algorithm 2 similarly produces a sample path under an inhomogeneous Markov chain.

Algorithm 1: `GibbsSample`$(x(0), \alpha, \beta, \sigma, h)$

input :

- $x(0)$ to specify the initial distribution $\delta_{x(0)}$,
- model parameters: α, β, σ,
- average number of hits per site: h

output : a sample path $\mathbf{x} = \big(x(0), x(1), \ldots, x(\lfloor hn^2 \rfloor) \big)$ from $\{X(j)\}_{j=0}^{\lfloor hn^2 \rfloor}$ given by (4) and (5).

initialize: $j \leftarrow 0$ and $\mathbf{x} \leftarrow (\, x(0)\,)$

for $j = 1, \ldots, \lfloor hn^2 \rfloor$ **do**

- $x(j) \leftarrow x(j-1)$
- pick a site s uniformly at random from $\mathbb{S}_n$
- $\theta \leftarrow \exp\big(-\big(\beta x_{N_s}(j) - (\sigma - \alpha)\big)\big)$
- $u \sim \text{Uniform}(0,1)$
- **if** $u \le \frac{1}{1+\theta}$ **then** $x_s(j) \leftarrow 1$ **else** $x_s(j) \leftarrow 0$;
- $\mathbf{x}$.`append`$(x(j))$

end

return x

Algorithm 2: `IGibbsSample`$(x(0), \alpha, \beta, \sigma(m), h)$

input :

- $x(0)$ to specify the initial distribution $\delta_{x(0)}$,
- model parameters: α, β,
- external stress function: $\sigma(m)$ for each time-block $m \in \{0, 1, 2, \ldots, M\}$,
- average number of hits per site per time-block m: h

output : a sample path $\mathbf{x} = \big(x(0), x(1), \ldots, x(M\lfloor hn^2 \rfloor) \big)$ from $\{X(j)\}_{j=0}^{M\lfloor hn^2 \rfloor}$ given by (8) and (7).

initialize: $m \leftarrow 0$ and $\mathbf{x} \leftarrow (\, x(0)\,)$

for $m = 0, 1, \ldots, M$ **do**

  for $i = 1, 2, \ldots, \underline{h} = \lfloor hn^2 \rfloor$ **do**

  - $j \leftarrow m\underline{h} + i$; $\quad x(j) \leftarrow x(j-1)$
  - pick a site s uniformly at random from $\mathbb{S}_n$
  - $\theta \leftarrow \exp\big(-\big(\beta x_{N_s}(j) - (\sigma(m) - \alpha)\big)\big)$
  - $u \sim \text{Uniform}(0,1)$
  - **if** $u \le \frac{1}{1+\theta}$ **then** $x_s(j) \leftarrow 1$ **else** $x_s(j) \leftarrow 0$;
  - $\mathbf{x}$.`append`$(x(j))$

  end

end

return x

References

[1] B. Y. Han, L. D. Sung, S. W. Kim, Biodegradable block copolymers as injectable drug-delivery systems, Nature 388 (1997) 860–862.

[2] Y. Qiu, K. Park, Environment-sensitive hydrogels for drug delivery, Advanced Drug Delivery Reviews 53 (2001) 321 – 339. Triggering in Drug Delivery Systems.

[3] Q. Hou, P. A. D. Bank, K. M. Shakesheff, Injectable scaffolds for tissue regeneration, J. Matter. Chem. 14 (2004) 1915.

[4] J. Beck, B. Madsen, D. Britt, B. Vernon, K. T. Nguyen, Islet encapsulation: Strategies to enhance islet cell functions, Tissue Engineering 13 (2007) 589–599.

[5] W. H. Herschel, R. Bulkley, Konsistenzmessungen von gummibenzollösungen, Kolloid-Zeitschrift 39 (1926) 291–300.

[6] W. Herschel, T. Bulkley, Measurement of consistency as applied to rubber¢benzene solutions, Am. Soc. Test Proc. 26(2) (1926) 621¢633.

[7] E. Bingham, Fluidity and Plasticity, McGraw-Hill, 1922.

[8] T. C. Papanastasiou, Flows of materials with yield, Journal of Rheology (1978-present) 31 (1987) 385–404.

[9] C. F. Möller, Peder, J. Mewis, D. Bonn, Yield stress and thixotropy: on the difficulty of measuring yield stress in practice, Soft Matter 2 (2006) 274–283.

[10] A. M. V. Putz, T. I. Burghelea, The solid-fluid transition in a yield stress shear thinning physical gel, Rheol Acta 48 (2009) 673–689.

[11] A. Poumaere, M. Moyers-Gonzlez, C. Castelain, T. Burghelea, Unsteady laminar flows of a carbopol gel in the presence of wall slip, Journal of Non-Newtonian Fluid Mechanics 205 (2014) 28 – 40.

[12] K. Dullaert, J. Mewis, A structural kinetics model for thixotropy, J. Non-Newtonian Fluid Mech. (2006) 21–30.

[13] D. Quemada, Rheological modeling of complex fluids: I:The concept of effective volume fraction revisited, Eur. Phys. J. AP (1998) 119–127.

[14] D. Quemada, Rheological modeling of complex fluids: III: Dilatant behaviour of stabilized suspensions, Eur. Phys. J. AP (1998) 309–320.

[15] D. Quemada, Rheological modeling of complex fluids: IV: Thixotropic and "thixoelastic" behaviour. Start-up and stress relaxation, creep tests and hysteresis cycles, Eur. Phys. J. AP (1999) 191–207.

[16] N. Roussel, R. Le Roy, P. Coussot, Thixotropy modelling at local and macrsocopic scales, J. non-Newtonian Fluid Mech. 117 (2004) 85–95.

[17] C. J. Dimitriou, R. H. Ewoldt, G. H. McKinley, Describing and prescribing the constitutive response of yield stress fluids using large amplitude oscillatory shear stress (laostress), Journal of Rheology (1978-present) 57 (2013) 27–70.

[18] F. Bautista, M. Munoz, J. Castillo-Tejas, J. H. Pérez-López, J. E. Puig, O. Manero, Critical phenomenon analysis of shear-banding flow in polymer-like micellar solutions. 1. theoretical approach, The Journal of Physical Chemistry B 113 (2009) 16101–16109. PMID: 19924843.

[19] W. Hong, X. Zhao, J. Zhou, Z. Suo, A theory of coupled diffusion and large deformation in polymeric gels, Journal of the Mechanics and Physics of Solids 56 (2008) 1779 – 1793.

[20] Y. An, F. J. Solis, H. Jiang, A thermodynamic model of physical gels, Journal of the Mechanics and Physics of Solids 58 (2010) 2083 – 2099.

[21] J. R. de Bruyn, Modeling the microrheology of inhomogeneous media, Journal of Non-Newtonian Fluid Mechanics 193 (2013) 21 – 27. Viscoplastic Fluids: From Theory to Application.

[22] F. K. Oppong, L. Rubatat, B. J. Frisken, A. E. Bailey, J. R. de Bruyn, Microrheology and structure of a yield-stress polymer gel, Phys. Rev. E 73 (2006) 041405.

[23] F. K. Oppong, J. R. de Bruyn, Diffusion of microscopic tracer particles in a yield-stress fluid, J. Non-Newtonian Fluid Mech. 142 (2007) 104–111.

[24] E. Ising, Beitrag zur theorie des ferromagnetismus, Zeitschrift für Physik 31 (1925) 253–258.

[25] E. H. Stanley, Phase transitions and critical phenomena, Oxford University Press, 1987.

[26] S. Slomkowski, J. V. Alemán, R. G. Gilbert, M. Hess, K. Horie, R. G. Jones, P. Kubisa, I. Meisel, W. Mormann, S. Penczek, R. F. T. Stepto, Terminology of polymers and polymerization processes in dispersed systems (iupac recommendations 2011), Pure and Applied Chemistry 83 (2011) 2229–2259.

[27] R. Jones, Compendium of polymer terminology and nomenclature IUPAC recommendations, 2008, Royal Society of Chemistry, Cambridge, 2009.

[28] D. Stauffer, A. Coniglio, M. Adam, Gelation and critical phenomena, Advances in Polymer Science 44 (1982) 103–158.

[29] P. Brémaud, Markov Chains: Gibbs Field, Monte carlo Simulation and Queues, Springer-Verlag, New York, 1999.

[30] O. Häggström, Finite Markov Chains and Algorithmic Applications, London Mathematical Society student texts, Cambridge University Press, 2002.

[31] T. M. Liggett, Interacting Particle Systems, Springer Berlin Heidelberg, 1985.

[32] B. Bollobás, O. Riordan, Percolation, Cambridge University Press, 2006.

[33] W. Hofschuster, W. Krämer, C-xsc 2.0: A c++ library for extended scientific computing, in: Numerical Software with Result Verification, pp. 15–35.

[34] J. R. de Bruyn, Modeling the microrheology of inhomogeneous media, Journal of Non-Newtonian Fluid Mechanics 193 (2013) 21–27.